

Simulation of Tau Decays in the Herwig++ Event Generator

David Grellscheid

*Institute of Particle Physics Phenomenology, Department of Physics
University of Durham, Durham, DH1 3LE, UK.*

Peter Richardson

*Institute of Particle Physics Phenomenology, Department of Physics
University of Durham, Durham, DH1 3LE, UK; and
Theoretical Physics Group, CERN, CH-1211, Geneva 23, Switzerland.*

Abstract

We describe the simulation of tau decays in the Herwig++ event generator, which includes sophisticated modelling of the hadronic currents and full treatment of spin correlation effects. The structure of the simulation makes it easy to add new models of tau decay, change the parameters of the existing models, and use the models from tau decay for the decay of other particles. The results are compared in detail with an existing simulation, and the benefits of the new structure are illustrated by considering the decay $\chi_1^\pm \rightarrow \chi_1^0 + \text{hadrons}$ in Anomaly-Mediated SUSY-Breaking (AMSB) models.

Key words: Monte Carlo Simulation, Tau Decays

PACS: 13.35.Dx, 14.60.Hi

1 Introduction

The use of Monte Carlo event generators is an essential part of all experimental analyses, both in interpreting data from existing experiments and in the design and planning of future experiments. The crucial role that Monte Carlo simulations play in experimental studies mean it is imperative these simulations are as accurate as possible.

Email addresses: david.grellscheid@durham.ac.uk (David Grellscheid), peter.richardson@durham.ac.uk (Peter Richardson).

While the existing Monte Carlo event generators have been highly successful over the last twenty years, a new generation of programs is necessary for the LHC. The reasons for this are twofold: a number of new ideas to improve the accuracy of the simulations have been suggested, *e.g.* [1,2,3,4,5], and the existing code structures required major redesign to allow new theoretical developments to be incorporated and to make long-term maintenance easier. Given the changing nature of computing in high energy physics, the natural choice is to write these new programs in C++. In preparation for the LHC a major effort is therefore underway to produce new versions of established simulations [6,7], as well as completely new event generators [8] in C++.

As part of the process of writing the new **Herwig++** event generator [7] we wish to improve many aspects of the simulation process. One area where major improvements are needed is in the simulation of tau lepton decays.

In FORTRAN HERWIG the τ decays were treated in the same way as the decays of the hadrons. The weak $V - A$ matrix element was used for the leptonic decays, and the other decays were generated using a phase-space distribution for the decay products. In addition, there were two interfaces to the specialised TAUOLA[9,10] package for τ decays. The first interface [1], which was part of HERWIG, was capable of generating longitudinal correlations in τ decays for all taus produced in the perturbative part of the event, while the second external interface [10] was capable of generating the longitudinal spin correlations of taus produced in W , Z/γ^* and H^\pm decays and the full correlation effects in neutral Higgs decays.

In **Herwig++** we wanted to:

- (1) include the matrix elements for τ decay as an integral part of the simulation, in order to both have a unified treatment of all decays and to remove the inherent problems in interfacing to external packages.¹
- (2) include the absent transverse spin correlations for all τ decays;
- (3) make it easy to change parameters in the hadronic currents used in the tau decays and the modelling of individual decay modes.

In this paper we will describe the simulation of τ decays in **Herwig++**. The aim of the simulation is to give a good description of tau decays with all the experimentally observed decay modes with branching ratio above the 5 per mille level included together with a reasonable model of the kinematics of the decay. Where possible we have used models which have been compared with, or tuned to, experimental data. In all cases the parameters of the models can be easily adjusted so that they can be tuned to new experimental data as it becomes available.

¹ In the FORTRAN simulation there were problems with the HERWIG interface due to changes in the TAUOLA program.

First we describe the factorization of the matrix element for τ decays and the structure of the code. This is followed by a description of the different models of the hadronic current which are used for the decay modes, together with comparisons with previous results. We then discuss our choice of models for the various τ decay modes. One major advantage of the new structure is that the hadronic currents can be used for applications other than τ decays which we illustrate by considering the weak decay of charginos to neutralinos in Anomaly-Mediated-SUSY Breaking (AMSB) models, where there is a small mass difference between the neutralino and chargino. Finally we present our conclusions.

2 Formalism

The matrix element for the decay of the τ lepton can be written as

$$\mathcal{M} = \frac{G_F}{\sqrt{2}} L_\mu J^\mu, \quad L_\mu = \bar{u}(p_{\nu_\tau}) \gamma_\mu (1 - \gamma_5) u(p_\tau), \quad (1)$$

where p_τ is the momentum of the τ and p_{ν_τ} is the momentum of the neutrino produced in the decay. The information on the decay products of the virtual W boson is contained in the hadronic current, J^μ . This factorization allows us to implement the leptonic current L_μ for the decaying tau and the hadronic current separately and then combine them to calculate the τ decay matrix element.

In `Herwig++` the most important part of the simulation of hadronic decays is handled by the `Decayer` class. This class is responsible for:

- (1) generating the kinematics of the decay products;
- (2) inserting the spin-unaveraged matrix element used to perform the decay and the wavefunctions² for the decay products into the `Herwig++` structure.

All of the τ decays are handled by the `TauDecayer` class. This class inherits from the `DecayIntegrator` class. The `DecayIntegrator` includes a sophisticated multi-channel integrator to perform the phase-space integration of the decay modes, leaving the implementation of the matrix element calculation and definition of the resonance structure of a multi-body decay mode the only tasks which need to be performed when implementing a new decay model.

The hadronic currents for a large range of modes are implemented as described

² In `Herwig++` these are the spinors and polarization vectors of the fermions and vector mesons.

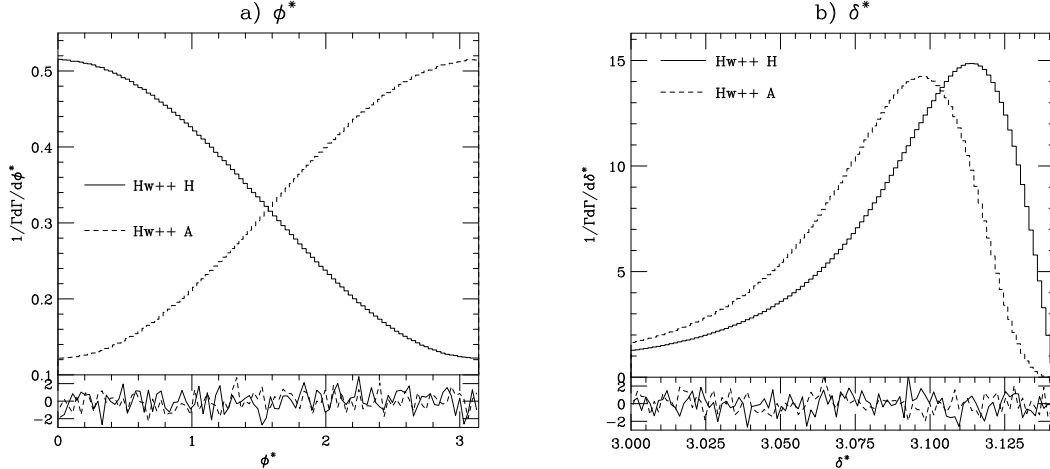


Fig. 1. Correlations between the decay products for $\{H, A\} \rightarrow \tau^+\tau^-$ followed by $\tau \rightarrow \pi\nu_\tau$ for a Higgs boson mass of 120 GeV. This plot shows the variables considered in [14]. Figure (a) shows the angle between the planes of the two tau decays and (b) shows the angle between the pions in the rest frame of the Higgs boson.

in Section 3. The classes implementing these currents all inherit from `WeakDecayCurrent`. The `TauDecayer` combines the hadronic current with its internal calculation of the leptonic current to compute the matrix element, and generates the momenta of the decay products using the features of its parent `DecayIntegrator` class for the generation of the phase space.

Given the spin-unaveraged matrix elements, the algorithm described in [11,12,13,1] is used in `Herwig++` to include spin correlation effects in all stages of the event generation process. The `Herwig++` structure, in particular the `DecayHandler` class, is responsible for passing the correct information between the `Decayer` objects in order to generate the spin correlations.

Examples of these correlations for the decay of scalar and pseudoscalar Higgs bosons to $\tau^+\tau^-$ followed by the decays of $\tau \rightarrow \pi\nu_\tau$ and $\tau \rightarrow \rho\nu_\tau$ are shown in Figures 1 and 2 respectively.³ In the absence of the correct correlations the ϕ^* distributions in both cases would be flat. The approach of [11,12,13,1] is in good agreement with the results of `TAUOLA` where the two methods can be compared⁴ but can generate the full correlations regardless of how the tau is produced.

³ In all the plots version 2.1 of `Herwig++` is compared with the `TAUOLA-PHOTOS` package of October 2005.

⁴ The full effects can only be compared in neutral Higgs decay as this is the only case in which `TAUOLA` implements the full correlations. However, there are many cases where the transverse correlations are not important and for which the two approaches are in good agreement, see for example Section 4.4 of [15].

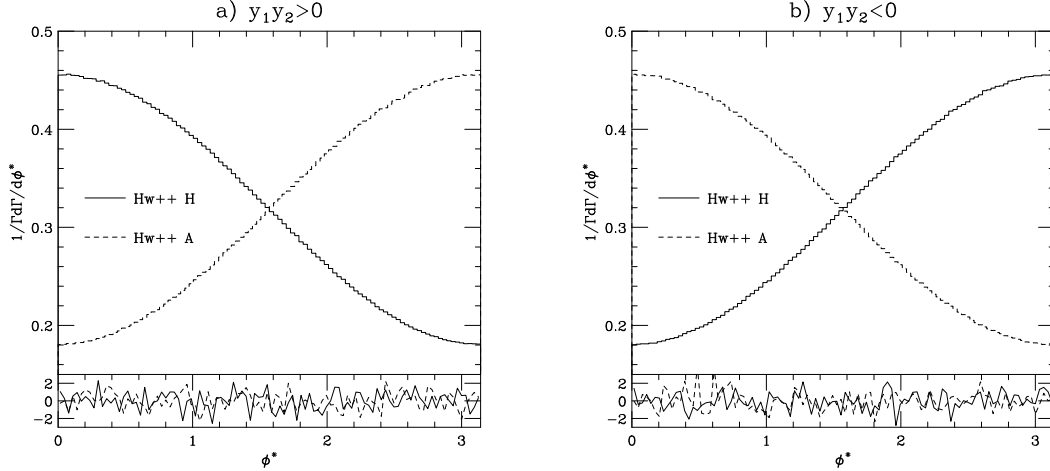


Fig. 2. Correlations between the decay products for $\{H, A\} \rightarrow \tau^+\tau^-$ followed by $\tau \rightarrow \rho\nu_\tau$ for a Higgs boson mass of 120 GeV. This plot shows the variables considered in [16]. The angle between the decay planes of the two ρ mesons in the $\rho^+\rho^-$ rest frame is shown for (a) $y_1y_2 > 0$ and (b) $y_1y_2 < 0$. The variables $y_{1,2}$ are defined in terms of the energies of the particles in the respective τ rest frames, $y_1 = \frac{E_{\pi^+} - E_{\pi^0}}{E_{\pi^+} + E_{\pi^0}}$ for the ρ^+ decay and $y_2 = \frac{E_{\pi^-} - E_{\pi^0}}{E_{\pi^-} + E_{\pi^0}}$ for the ρ^- decay.

In Figures 1 and 2, and all subsequent, figures the TAUOLA result is not shown as it is virtually indistinguishable from the Herwig++ result due to the high statistics used. Similarly where present the lower panel shows the difference between the TAUOLA [9] and Herwig++ results in terms of the statistical error for mass distributions, and the fractional difference for running widths.

3 Hadronic Currents

We have implemented a wide range of models for the weak hadronic currents. The various models are described in this section together with comparisons with the results of TAUOLA, where appropriate.

3.1 Pseudoscalar Meson

The simplest hadronic current is that for the production of a pseudoscalar meson, *e.g.* the current for the production of π^\pm in the decay of the tau. The hadronic current can be written as

$$J^\mu = f_P p_P^\mu, \quad (2)$$

Mode	Herwig++ $\Gamma_{\text{partial}}/10^{-13} \text{ GeV}$	TAUOLA $\Gamma_{\text{partial}}/10^{-13} \text{ GeV}$	Difference $/10^{-17} \text{ GeV}$
PseudoScalar Meson			
π^-	2.4334	2.4334	0
K^-	0.16611	0.16611	0
Two PseudoScalar Mesons via Intermediate Vector Mesons			
$\pi^- \pi^0$	5.3998 ± 0.0002	5.3998 ± 0.0002	0 ± 3
$K^- \pi^0$	0.081295 ± 0.000002	0.081293 ± 0.000001	0.02 ± 0.03
$\bar{K}^0 \pi^-$	0.156196 ± 0.000004	0.156195 ± 0.000003	0.01 ± 0.04
$K^- K^0$	0.0024248 ± 0.000001	0.0024251 ± 0.000001	-0.03 ± 0.02
$K\pi$ via Intermediate Scalar and Vector Mesons			
$K^- \pi^0$	0.081292 ± 0.000003	0.081293 ± 0.000001	-0.01 ± 0.04
$\bar{K}^0 \pi^-$	0.156200 ± 0.000005	0.156195 ± 0.000003	0.05 ± 0.06
Charged Lepton and Neutrino			
$e^- \nu_e$	4.0491 ± 0.0002	4.0492 ± 0.0002	-1 ± 3
$\mu^- \nu_\mu$	3.9380 ± 0.0002	3.9380 ± 0.0002	0 ± 3

Table 1

Partial widths for two- and three-body decay modes of the τ calculated with Herwig++ and TAUOLA. In order to compare the results of Herwig++ with TAUOLA, the masses of the decay products in TAUOLA were adjusted to the Herwig++ values, as were the pion and kaon decay constants and the Cabibbo angle. For the two meson, via intermediate vector mesons, decays the parameters of the resonances in the form-factors in Herwig++ were set to those used in TAUOLA, the CPC version was used for the $\pi^- \pi^0$ and $K^- K^0$ modes and the CLEO version for the $K\pi$ modes. For the $K\pi$ modes including scalar resonances a transverse form of the projection operator was used together with the resonance parameters from the CLEO version of TAUOLA in Herwig++. In the leptonic decays the radiative corrections in TAUOLA were switched off. For the $K\pi$ and $K^- K^0$ modes our choice of the normalisation was used.

where p_P^μ is the momentum of the pseudoscalar meson and f_P is the pseudoscalar meson decay constant.

The partial widths for the decays $\tau^- \rightarrow \pi^- \nu_\tau$ and $\tau^- \rightarrow K^- \nu_\tau$ are given in Table 1 and agree with those from TAUOLA. Another important check is that the spin correlation effects are correctly implemented. The correlations in Higgs decays followed by the decay of the tau to a single pion are shown in Fig. 1 and are in excellent agreement with the results of TAUOLA.

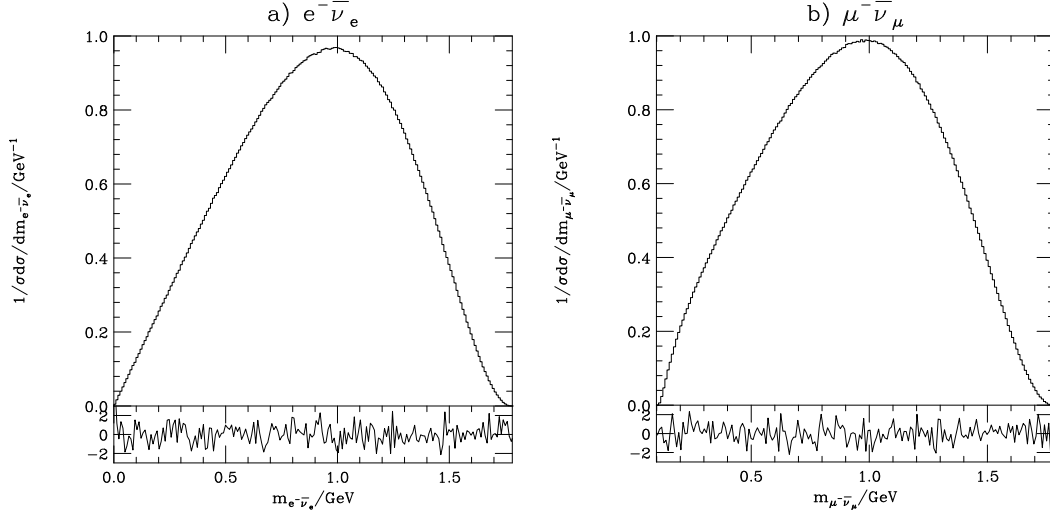


Fig. 3. The differential decay rate with respect to the mass of the lepton-neutrino pair for $\tau^- \rightarrow \ell^- \bar{\nu}_\ell \nu_\tau$. The TAUOLA result was generated with the radiative corrections switched off.

3.2 Vector Meson

The current for the production of a vector meson is given by

$$J^\mu = \sqrt{2} g_V \epsilon_V^{*\mu}, \quad (3)$$

where $\epsilon_V^{*\mu}$ is the polarization vector for the outgoing meson and g_V is the decay constant of the vector meson.

This current was included to test some aspects of the spin correlations, test the treatment of off-shell effects and for future extensions, but is not used in tau decays because all such decays are better modeled by a complete description of the the production and decay of the vector meson as implemented in the various models described below.

3.3 Charged Lepton and Neutrino

The current for weak decay to a lepton and the associated anti-neutrino is given by

$$J^\mu = \bar{u}(p_\ell) \gamma^\mu (1 - \gamma_5) v(p_{\bar{\nu}}), \quad (4)$$

where $p_{\bar{\nu}}$ is the momentum of the anti-neutrino and p_ℓ is the momentum of the charged lepton.

The mass distribution of the $\ell^- \bar{\nu}_\ell$ produced in the decay $\tau^- \rightarrow \ell^- \bar{\nu}_\ell \nu_\tau$ is shown in Fig. 3. As can be seen there is good agreement between **Herwig++** and

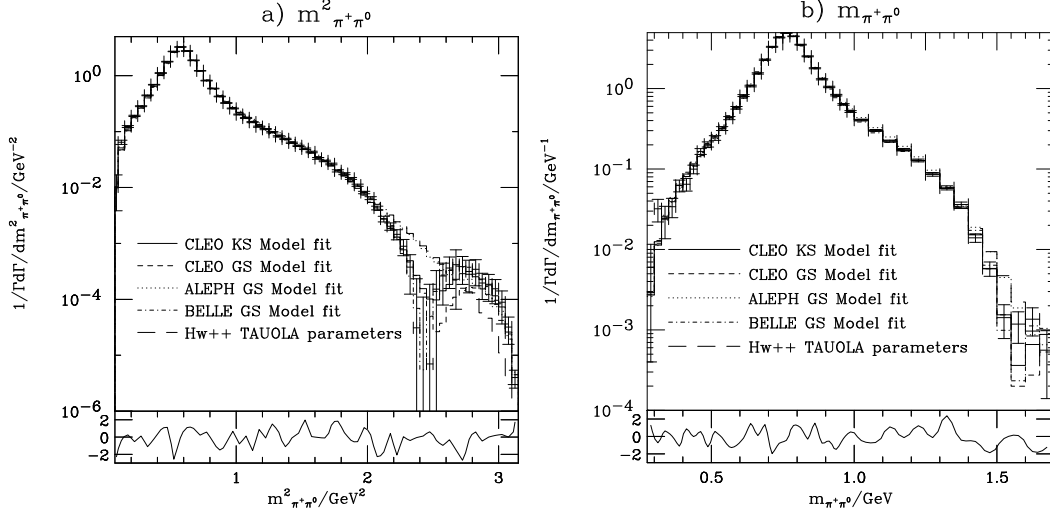


Fig. 4. The mass spectrum for $\pi^-\pi^0$ in the decay $\tau \rightarrow \pi^-\pi^0\nu_\tau$. a) shows $m_{\pi^-\pi^0}^2$ compared with CLEO data taken from [19] and b) shows $m_{\pi^-\pi^0}$ compared with Belle data from [20]. The results of Herwig++ using the form-factor parameters from the fits of CLEO [19], Belle [20] and ALEPH [21] are shown together with the result from Herwig++ using the TAUOLA parameters.

TAUOLA in terms of both the differential distributions and the partial widths given in Table 1. For these comparisons the masses of the particles in TAUOLA were set to the Herwig++ values and the radiative corrections switched off.

In general we have not yet considered radiative corrections to tau decays in Herwig++. However, we do have a treatment of electromagnetic radiation in $1 \rightarrow 2$ decays [17] based on the YFS formalism [18] which resums the dominant soft radiation to all orders and treats the universal large collinear logarithms. This can be applied to τ decays in the approximation that the decay is treated as a series of $1 \rightarrow 2$ processes, which is reasonable for many of the decay modes. The YFS formalism can be systematically improved to incorporate exact, process specific, higher order corrections so in the future we can extend this simulation to include the full radiative corrections in tau decay.

3.4 Two Pseudoscalar Mesons via Intermediate Vector Mesons

The weak current for the production of two mesons via the ρ or K^* resonances has the form

$$J^\mu = (p_1 - p_2)_\nu \left(g^{\mu\nu} - \frac{q^\mu q^\nu}{q^2} \right) \frac{W}{\sum_k \alpha_k} \sum_k \alpha_k B_k(q^2), \quad (5)$$

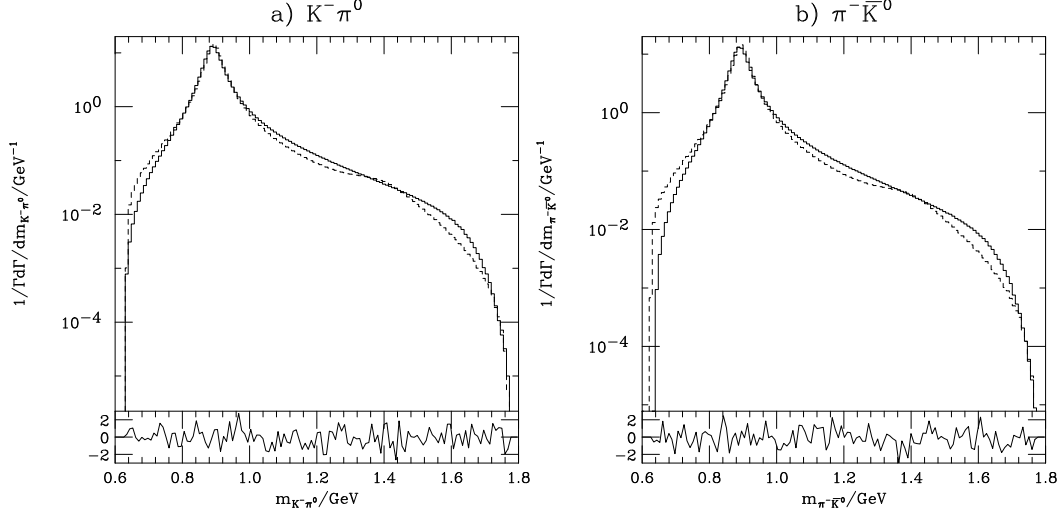


Fig. 5. The mass spectrum of a) $K^-\pi^0$ and b) $\pi^-\bar{K}^0$. In a) the solid line is the result of the model described in Section 3.4 using the TAUOLA parameters for the form-factor and in b) the solid line is the result of the model described in Section 3.5 with no scalar component, using with a transverse form of the projection operator and the parameters of the vector form factor set to the TAUOLA values. In both plots the dashed line was generated using the model from Section 3.5 using the fit of [24].

where $p_{1,2}$ are the momenta of the outgoing mesons, $q = p_1 + p_2$, $B_k(q^2)$ is the Breit-Wigner distribution for the intermediate vector meson k and α_k is the weight for the resonance. The Breit-Wigner terms are summed over the ρ or K^* resonances that can contribute to a given decay mode.

The models of either Kühn and Santamaria [22], which uses a Breit-Wigner distribution with a p-wave running width Eqn. A.2, or Gounaris and Sakurai [23], which uses the form given in Eqn. A.4, are supported for the shape of the Breit-Wigner distribution.

The following decay modes: $\rho^- \rightarrow \pi^-\pi^0$; $K^{*-} \rightarrow K^-\pi^0$; $K^{*-} \rightarrow \bar{K}^0\pi^-$; $\rho^- \rightarrow K^-K^0$; $K^{*-} \rightarrow K^-\eta$ are supported with weights, W : $\sqrt{2}$; $\frac{1}{\sqrt{2}}$; 1; 1; $\sqrt{\frac{3}{2}}$. respectively. ⁵

There has been a number of recent studies of the $\pi^\pm\pi^0$ mode [19,21,20]. The fits from these studies are compared with the data from CLEO [19] and Belle [20] in Fig. 4 together with a comparison of the results of Herwig++ and TAUOLA. The partial width using the TAUOLA parameters is compared with that from TAUOLA in Table 1. The CLEO, ALEPH and Belle fits differ in the amount

⁵ It should be noted that this normalisation for the $K\pi$ and KK modes is different from that in TAUOLA [9,10]. However, it agrees with that of [25] for the $K\pi$ modes and [26] for the $K\eta$ mode.

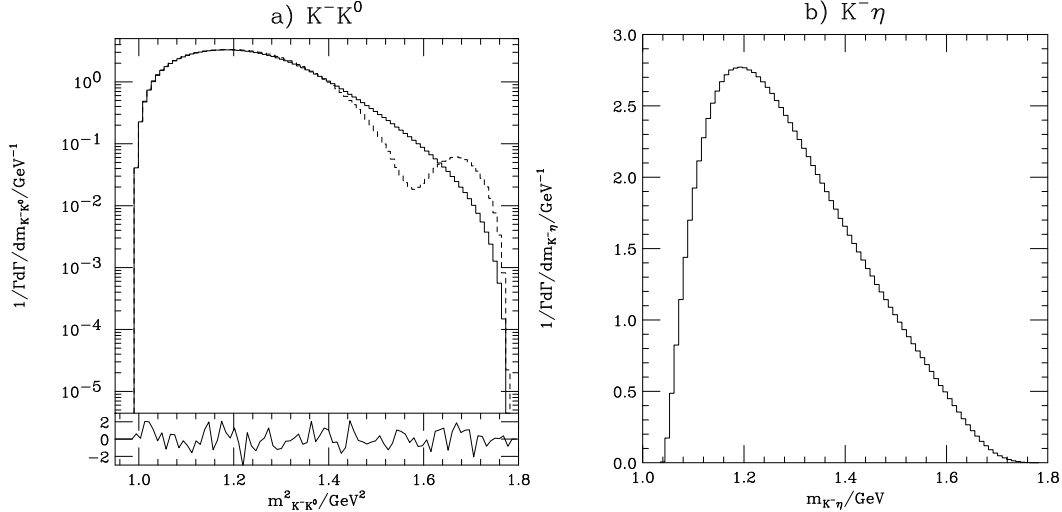


Fig. 6. The mass spectrum for a) $K^- K^0$ and b) $K^- \eta$. For the $K^- K^0$ spectrum the solid lines were generated using the parameters from the CPC version of TAUOLA for the form factor while the dashed line uses the default Herwig++ parameters for the rho form factor.

of the $\rho(1700)$ resonance which is present, giving destructive interference in the high mass region. We have therefore chosen to use the parameters of the CLEO fit using the model of Kühn and Santamaria [22], which lies between the ALEPH and Belle fits, as our default choice.

There have been a number of recent studies of the $K\pi$ modes [27,28,24] which favour a low-mass enhancement and little contribution of the $K^*(1410)$. We have therefore chosen use a model which includes scalar resonances, as described in Section 3.5, by default for the $K\pi$ modes. For this model we use same parameters as the CLEO version of TAUOLA, which includes the $K^*(892)$ and $K^*(1680)$ resonances. The mass spectrum for the $K^+\pi^0$ mode shown in Fig. 5a shows good agreement between Herwig++ and TAUOLA, as does the partial width for the $K\pi$ modes given in Table 1.

The mass spectrum for $K^- K^0$ generated by Herwig++ is compared with that generated by TAUOLA in Fig. 6a, again there is good agreement between Herwig++ and TAUOLA for both the shape of the distribution and the partial width for the decay mode given in Table 1. The spectrum for the $K\eta$ mode is shown in Fig. 6b.

3.5 $K\pi$ via Intermediate Scalar and Vector Mesons

Unlike the $\pi^+\pi^0$ decay of the tau the $K\pi$ decay mode can occur via either intermediate scalar or vector mesons. We therefore include a model for the

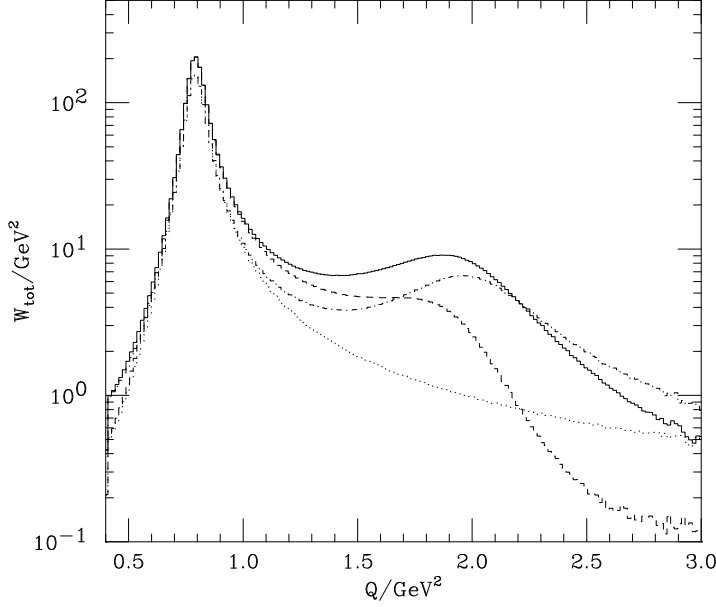


Fig. 7. The hadronic structure function W_{tot} for $\tau \rightarrow K\pi\nu_\tau$. The solid black line shows the result with the default parameters of [29], the short dashed line shows the result without the scalar contribution, the dot-dashed line shows the result without the $K^*(1410)$ and the dotted line shows the result with neither the $K^*(1410)$ or scalar contribution. This plot is the equivalent of Fig.1a of [29].

current for the $K\pi$ decay mode including the contribution of both vector and scalar resonances based on the model of [29]. The current is given by

$$J^\mu = c_V(p_1 - p_2)_\nu \frac{1}{\sum_k \alpha_k} \sum_k \alpha_k \text{BW}_k(q^2) \left(g^{\nu\mu} - \frac{q^\nu q^\mu}{M_k^2} \right) + c_S q^\mu \frac{1}{\sum_k \beta_k} \sum_k \beta_k \text{BW}_k(q^2), \quad (6)$$

where $p_{1,2}$ are the momenta of the outgoing mesons, $q = p_1 + p_2$, $\text{BW}_k(q^2)$ is the Breit-Wigner distribution for the intermediate mesons and α_k is the weight for the resonance. The sum over the resonances is over the vector K^* states in the first, vector, part of the current and the excited scalar K^* resonances in the second, scalar, part of the current. By default the vector part of the current includes the $K^*(892)$ and $K^*(1410)$ states and the scalar part of the current includes the $K_0^*(1430)$ together with the option of including the $\kappa(800)$ to model any low-mass enhancement in the mass of the $K\pi$ system, although additional resonances can be included if necessary.

The mass spectrum for the $\pi^- \bar{K}^0$ mode is shown in Fig. 5b, where the parameters have been chosen to give the same form factor as TAUOLA. There is good agreement with TAUOLA for both the shape of the distribution and the partial widths, which are given in Table 1.

The results for the hadronic structure function defined in [29] are shown in Fig. 7 for different values of the parameters. This shows good agreement with

Fig.1a of [29], upon which it is based. The branching ratios for the different parameters values are also in good agreement with the results of [29].

The most recent study [24] of the $K\pi$ mass spectrum sees a low-mass enhancement which is modelled using the scalar κ resonance. By default we use a set of parameters this model which reproduces the fit of [24] to the mass spectrum with the κ , $K^*(892)$ and $K^*(1410)$ resonances, as shown in Fig. 5 for both the $K^-\pi^0$ and $\pi^-\bar{K}^0$ mass distributions. The low-mass enhancement due to the κ can clearly be seen in these distributions.

3.6 Three Pseudoscalar Mesons

In order to simplify the implementation of a number of standard currents for the production of three pseudoscalar mesons we define the current in terms of a number of form factors. The current is defined to be [9]

$$J^\mu = \left(g^{\mu\nu} - \frac{q^\mu q^\nu}{q^2} \right) [F_1(p_2 - p_3)^\mu + F_2(p_3 - p_1)^\mu + F_3(p_1 - p_2)^\mu] \quad (7)$$

$$+ q^\mu F_4 + iF_5 \epsilon^{\mu\alpha\beta\gamma} p_1^\alpha p_2^\beta p_3^\gamma,$$

where $p_{1,2,3}$ are the momenta of the mesons in the order given below and $F_{1\rightarrow 5}$ are the form factors. We use this approach for a number of three meson modes which occur in τ decays: $\pi^-\pi^-\pi^+$; $\pi^0\pi^0\pi^-$; $K^-\pi^-K^+$; $K^0\pi^-\bar{K}^0$; $K^-\pi^0K^0$; $\pi^0\pi^0K^-$; $K^-\pi^-\pi^+$; $\pi^-\bar{K}^0\pi^0$; $\pi^-\pi^0\eta$; $K_S^0\pi^-K_S^0$; $K_L^0\pi^-K_L^0$; $K_S^0\pi^-K_L^0$. The current is implemented in terms of these form factors in a base class so that any model for these currents can be implemented by inheriting from this class and specifying the form factors.

We currently implement three models for these decays, the general model of [22,30,9] which treats all the decay modes, the model of CLEO [31] for the three-pion modes and the model of [25] for the kaon modes.

3.6.1 General Model

This is the implementation of the model [22,30,9] which uses the form of [22] for the a_1 width. The form factors for the different modes are given in [30,9]. A Breit-Wigner distribution, Eqn. A.2, with a running width is used for the a_1 . As the dominant decay of a_1 is to three pions, a more complicated form of the running width is used. A parameterisation of the energy dependence of the running width is given [22] for the default parameter values for the ρ form factor. Instead of using this parameterisation we calculate an interpolation table for the running width at initialisation with the actual ρ form-factor

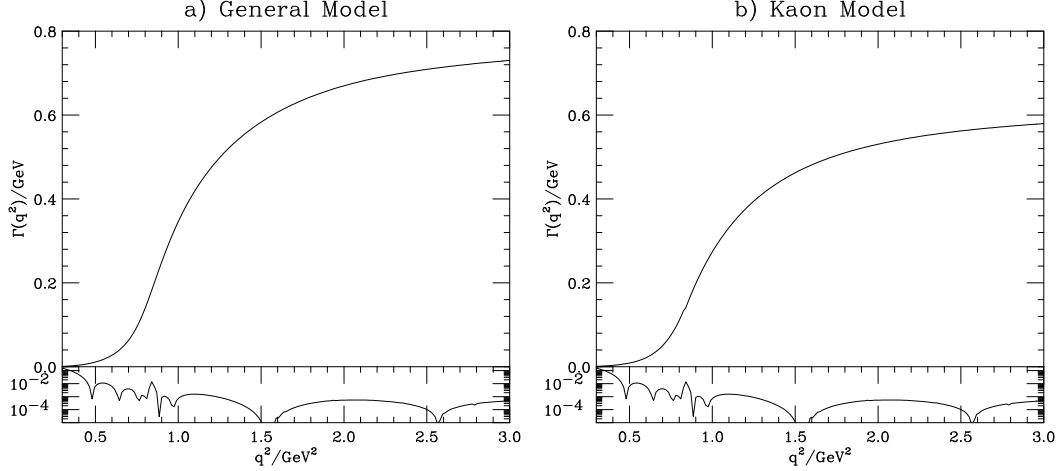


Fig. 8. The running a_1 width calculated using the model of [22]. a) shows the running width for the parameters used in the Section 3.6.1 and b) shows the running width for the parameters used in the Section 3.6.3. The result from numerically evaluating the matrix element in **Herwig++** is shown.

parameters. Our calculation of the running width is compared with the result of [22] in Fig. 8; there is good agreement between the two results.

The results for the partial widths for all the modes are compared with the results from **TAUOLA** in Table 2 which shows good agreement between the two programs. The mass distributions for the hadronic system and the $\pi^+\pi^-$ subsystem, which contains the ρ resonance, for the $\tau^- \rightarrow \pi^-\pi^-\pi^+\nu_\tau$ mode are shown in Fig. 9. The mass distributions of the $\pi^0\pi^0\pi^-$ system and the $\pi^-\pi^0$ system are shown in Fig. 10, for the $\tau^- \rightarrow \pi^0\pi^0\pi^-\nu_\tau$ mode.

The mass distributions of the $K^-\pi^-K^+$ system and the π^-K^+ system are shown in Fig. 11 for the $\tau^- \rightarrow K^-\pi^-K^+\nu_\tau$ decay mode. The mass distributions of the $K^0\pi^-\bar{K}^0$ hadronic system and the $\pi^-\bar{K}^0$ system are shown in Fig. 12 for the $\tau^- \rightarrow K^0\pi^-\bar{K}^0\nu_\tau$ decay mode. The mass distributions of the hadronic system and the $K^-\pi^0$ subsystem are shown in Fig. 13 for the $\tau^- \rightarrow K^-\pi^0K^0\nu_\tau$ decay mode.

The mass distributions of the hadronic system and the π^0K^- subsystem are shown in Fig. 14 for the decay mode $\tau^- \rightarrow \pi^0\pi^0K^-\nu_\tau$. The mass distributions of the $K^-\pi^+\pi^-$ system and $\pi^+\pi^-$ subsystem are shown in Fig. 15 for the decay $\tau^- \rightarrow K^-\pi^+\pi^-\nu_\tau$. The mass distributions of the $\pi^-\bar{K}^0\pi^0$ system and the $\pi^-\bar{K}^0$ subsystem are shown in Fig. 16 for the decay $\tau^- \rightarrow \pi^-\bar{K}^0\pi^0\nu_\tau$.

Finally the mass distributions of the $\pi^-\pi^0\eta$ system and the $\pi^-\pi^0$ subsystem are shown in Fig. 17 for the $\tau^- \rightarrow \pi^-\pi^0\eta\nu_\tau$ decay. It should be noted that this mode is very sensitive to the value of the η mass used.

In all cases there is good agreement between **Herwig++** and **TAUOLA**.

Mode	Herwig++ $\Gamma_{\text{partial}}/10^{-13} \text{ GeV}$	TAUOLA $\Gamma_{\text{partial}}/10^{-13} \text{ GeV}$	Difference $/10^{-17} \text{ GeV}$
General Model			
$\pi^- \pi^- \pi^+$	1.4632 ± 0.0001	1.4633 ± 0.0001	-1 ± 1
$\pi^- \pi^0 \pi^0$	1.4957 ± 0.0001	1.4958 ± 0.0001	-1 ± 1
$K^- \pi^- K^+$	$(2.4567 \pm 0.0003) \times 10^{-2}$	$(2.4572 \pm 0.0001) \times 10^{-2}$	-0.05 ± 0.03
$K^0 \pi^- \bar{K}^0$	$(2.2694 \pm 0.0002) \times 10^{-2}$	$(2.2696 \pm 0.0001) \times 10^{-2}$	-0.02 ± 0.03
$K^- \pi^0 \bar{K}^0$	$(2.0877 \pm 0.0001) \times 10^{-3}$	$(2.0878 \pm 0.0001) \times 10^{-3}$	-0.001 ± 0.002
$\pi^0 \pi^0 K^-$	$(2.5421 \pm 0.0003) \times 10^{-2}$	$(2.5419 \pm 0.0001) \times 10^{-2}$	0.03 ± 0.03
$K^- \pi^- \pi^+$	0.13077 ± 0.00001	0.13078 ± 0.00001	-0.1 ± 0.2
$\pi^- \bar{K}^0 \pi^0$	0.13204 ± 0.00002	0.13201 ± 0.00001	0.3 ± 0.2
$\pi^- \pi^0 \eta$	$(4.6175 \pm 0.0009) \times 10^{-2}$	$(4.6160 \pm 0.0008) \times 10^{-2}$	0.15 ± 0.12
CLEO model for Three Pions			
$\pi^- \pi^- \pi^+$	1.2605 ± 0.0001	1.2604 ± 0.0001	1 ± 1
$\pi^- \pi^0 \pi^0$	1.2702 ± 0.0001	1.2702 ± 0.0001	0 ± 1
Two Pions and a Photon			
$\pi^- \pi^0 \gamma$	$(1.2708 \pm 0.0001) \times 10^{-2}$	$(1.2707 \pm 0.0001) \times 10^{-2}$	0.01 ± 0.01
4 pions			
$2\pi^- \pi^0 \pi^+$	0.95120 ± 0.00009	0.95112 ± 0.00006	0.8 ± 1.1
$3\pi^0 \pi^-$	0.24453 ± 0.0002	0.24452 ± 0.0002	0.1 ± 2
5 pions			
$\pi^- 4\pi^0$	$(3.6192 \pm 0.0010) \times 10^{-2}$	$(3.6185 \pm 0.0007) \times 10^{-2}$	0.07 ± 0.12
$3\pi^- 2\pi^+$	$(4.2745 \pm 0.0010) \times 10^{-2}$	$(4.2746 \pm 0.0006) \times 10^{-2}$	-0.01 ± 0.12
$2\pi^- 2\pi^0 \pi^+$	$(1.1883 \pm 0.0004) \times 10^{-1}$	$(1.1884 \pm 0.0003) \times 10^{-1}$	-0.1 ± 0.5

Table 2

The partial widths for the three-, four- and five-meson decay modes of the τ calculated using Herwig++ and TAUOLA. In order to compare the results of the two programs, the masses of the decay products in TAUOLA were set to the Herwig++ values, as was the Cabibbo angle. For the five pion decays the ρ form factors were not included in the decay of the ω .

3.6.2 CLEO Model for Three Pions

This is the implementation of the model of [31] for the weak current for three pions. This model includes ρ mesons in both the s- and p-wave, the scalar σ resonance, the tensor f_2 resonance and scalar $f_0(1370)$. The form factors for the $\pi^0 \pi^0 \pi^-$ mode are given in [31] and the others can be obtained by isospin rotation.

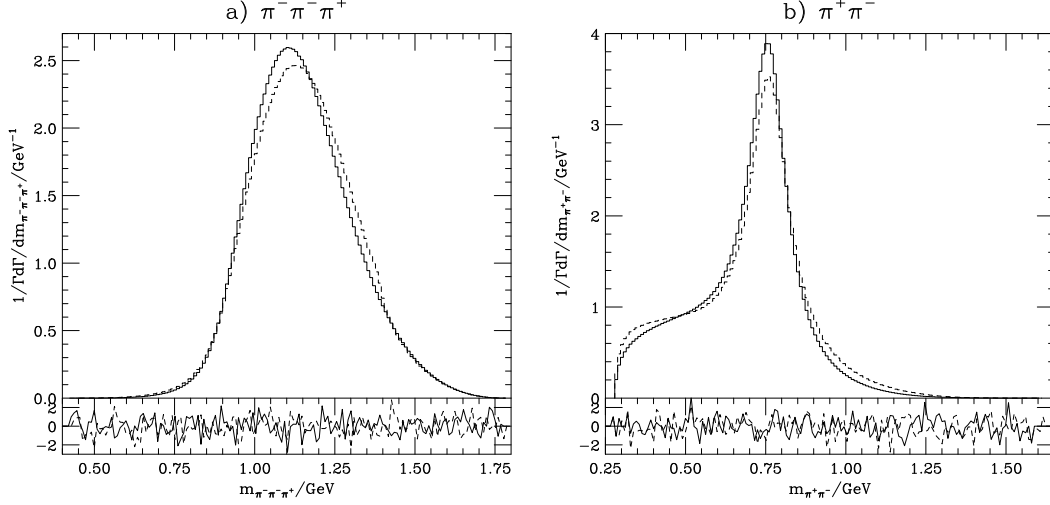


Fig. 9. Differential distribution for the mass of a) $\pi^- \pi^- \pi^+$ and b) $\pi^+ \pi^-$ produced in the decay $\tau^- \rightarrow \pi^- \pi^- \pi^+ \nu_\tau$. The solid line is the model of [9,22,30] and the dashed line that of [31].

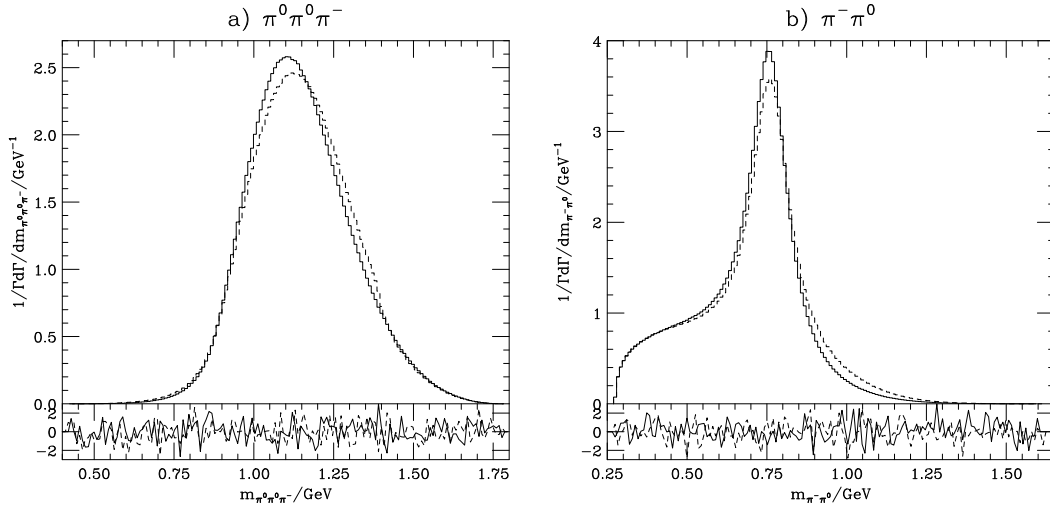


Fig. 10. Differential distribution for the mass of a) $\pi^0 \pi^0 \pi^-$ and b) $\pi^- \pi^0$ produced in the decay $\tau^- \rightarrow \pi^0 \pi^0 \pi^- \nu_\tau$. The solid line is the model of [9,22,30] and the dashed line that of [31].

In this case the running width for the a_1 is calculated using the current for the $\pi^- \pi^- \pi^0$ and $\pi^0 \pi^0 \pi^-$ modes of the a_1 together with an s-wave KK^* contribution. The running width is shown in Fig. 18a for the default parameter values and our calculation is in good agreement with that in TAUOLA.

The partial widths for the $\tau^- \rightarrow \pi^- \pi^- \pi^+ \nu_\tau$ and $\tau^- \rightarrow \pi^0 \pi^0 \pi^- \nu_\tau$ are compared with those from the CLEO version of TAUOLA in Table 2. The mass distributions of the $\pi^- \pi^- \pi^+$ system and the $\pi^+ \pi^-$ subsystem for the $\tau^- \rightarrow \pi^- \pi^- \pi^+ \nu_\tau$ are shown in Fig. 9. The mass distributions of the hadronic system and the $\pi^- \pi^0$ subsystem for the $\tau^- \rightarrow \pi^0 \pi^0 \pi^- \nu_\tau$ decay are shown in Fig. 10. There is

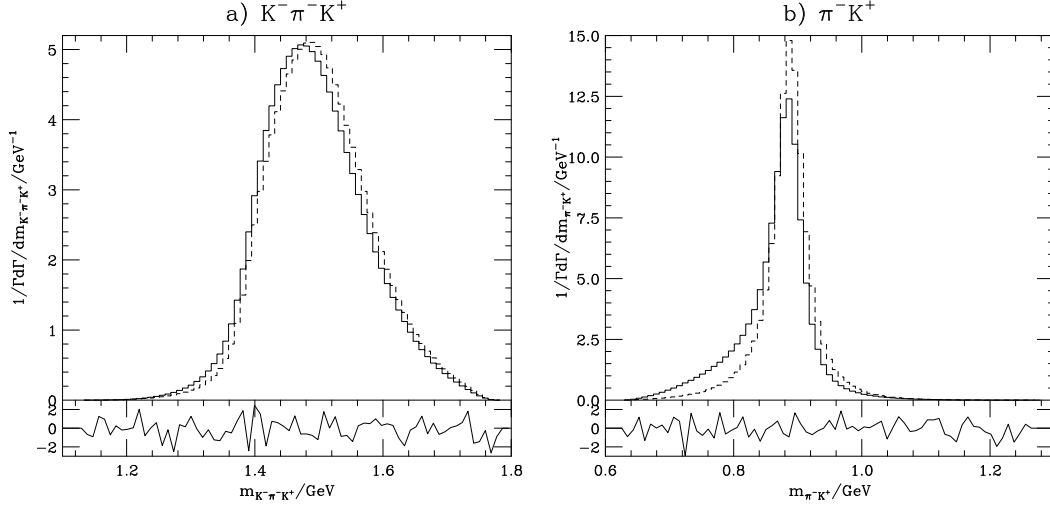


Fig. 11. Differential distribution for the mass of a) $K^- \pi^- K^+$ and b) $\pi^- K^+$ produced in the decay $\tau^- \rightarrow K^- \pi^- K^+ \nu_\tau$. The solid line is the model of [9,30] and the dashed line that of [25].

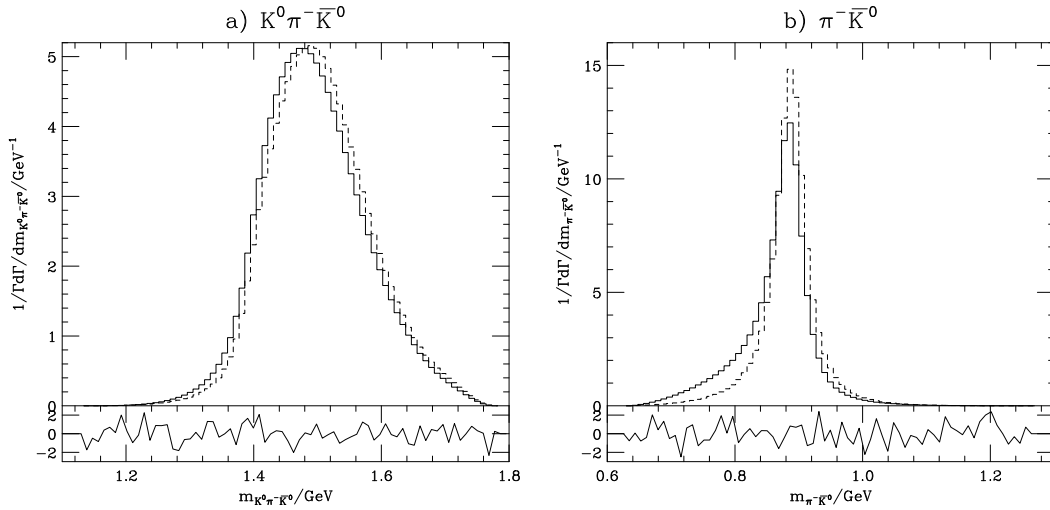


Fig. 12. Differential distribution for the mass of a) $K^0 \pi^- \bar{K}^0$ and b) $\pi^- \bar{K}^0$ produced in the decay $\tau^- \rightarrow K^0 \pi^- \bar{K}^0 \nu_\tau$. The solid line is the model of [9,30] and the dashed line that of [25].

good agreement with TAUOLA for this model which in general gives a higher mass for the hadronic system and a slightly broader distribution for the masses of the subsystems which include a rho resonance than the model of [9,22,30].

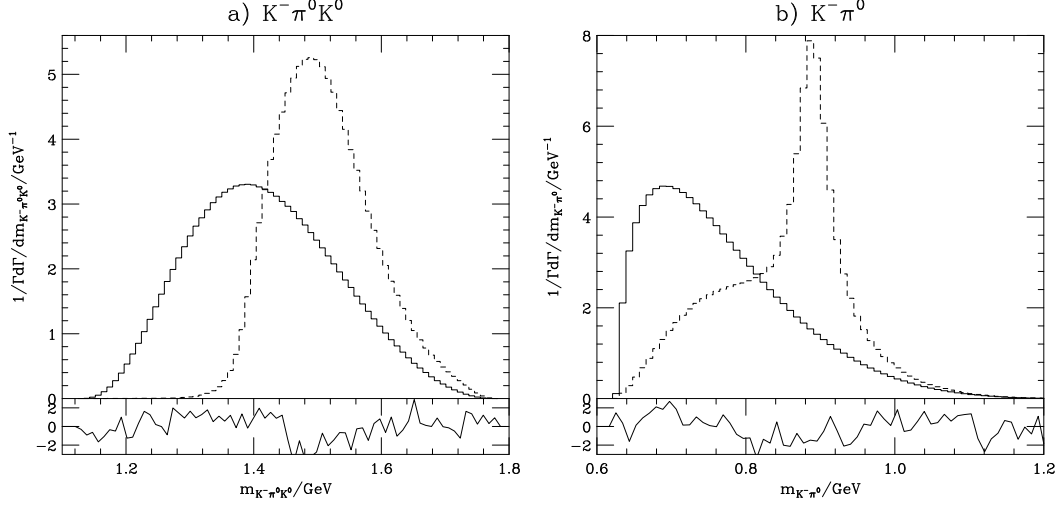


Fig. 13. Differential distribution for the mass of a) $K^-\pi^0K^0$ and b) $K^-\pi^0$ produced in the decay $\tau^- \rightarrow K^-\pi^0K^0\nu_\tau$. The solid line is the model of [9,30] and the dashed line that of [25].

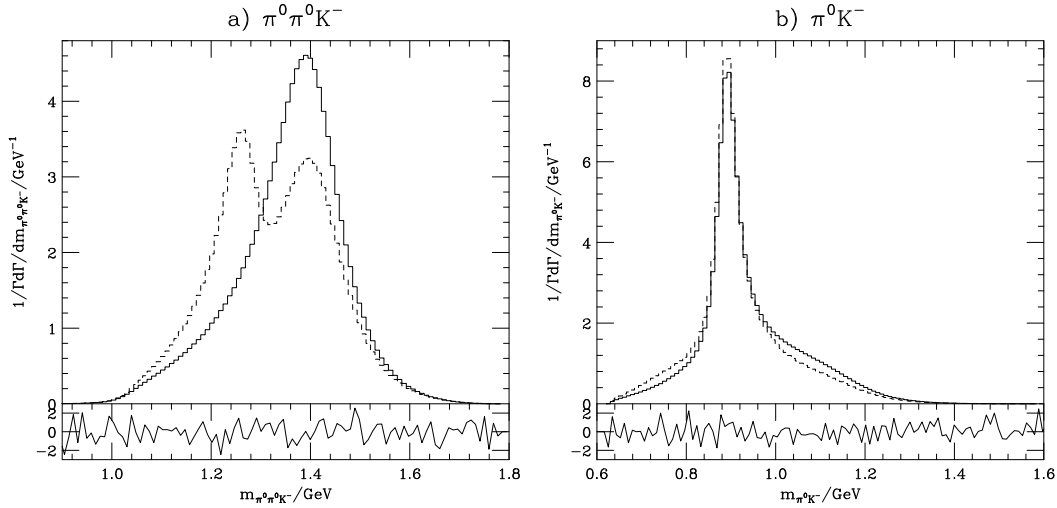


Fig. 14. Differential distribution for the mass of a) $\pi^0\pi^0K^-$ and b) π^0K^- produced in the decay $\tau \rightarrow \pi^0\pi^0K^-\nu_\tau$. The solid line is the model of [9,30] and the dashed line that of [25].

3.6.3 Model for modes including Kaons

Like the model of [30] the model of [25] is designed to reproduce the correct chiral limit for tau decays to three mesons. However, this model makes a different choice of the resonances to use away from this limit for the decays involving at least one kaon and in the treatment of the K_1 resonances.

The form factors for the different modes are given in [25]. The same form of the a_1 Breit-Wigner is used as in Section 3.6.1, with the mass and width taken from [25]. The running width we calculate using this model with this

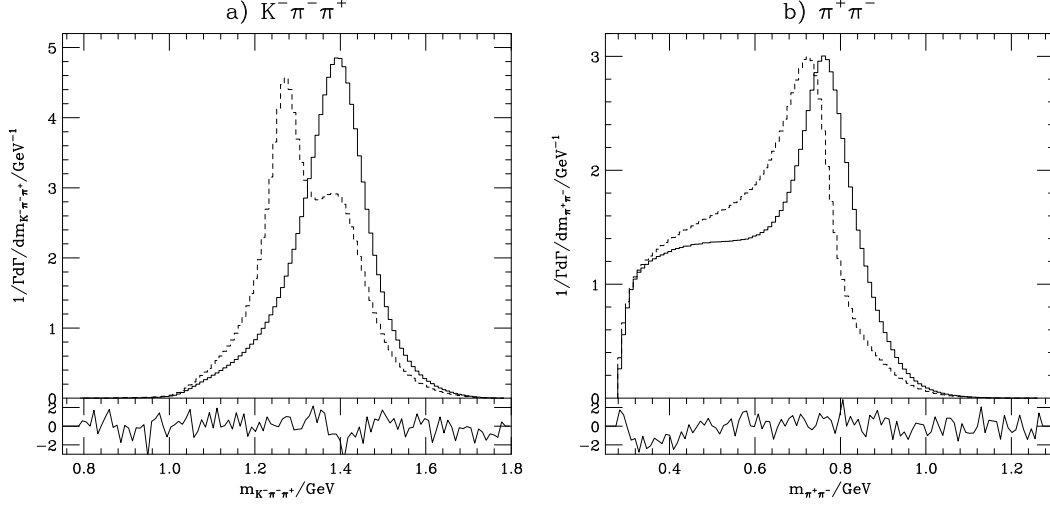


Fig. 15. Differential distribution for the mass of a) $K^- \pi^- \pi^+$ and b) $\pi^+ \pi^-$ produced in the decay $\tau^- \rightarrow K^- \pi^- \pi^+ \nu_\tau$. The solid line is the model of [9,30] and the dashed line that of [25].

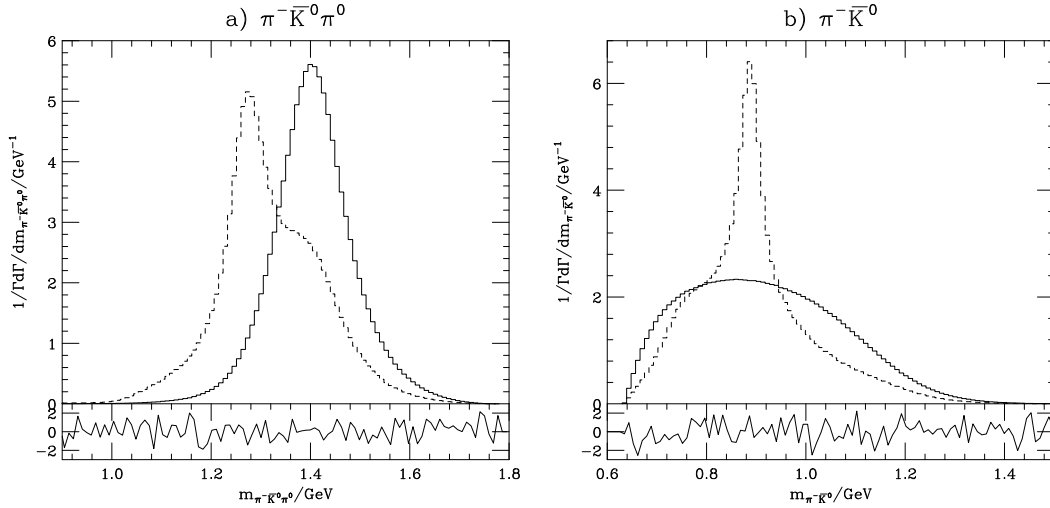


Fig. 16. Differential distribution for the mass of a) $\pi^- \bar{K}^0 \pi^0$ and b) $\pi^- \bar{K}^0$ produced in the decay $\tau^- \rightarrow \pi^- \bar{K}^0 \pi^0 \nu_\tau$. The solid line is the model of [9,30] and the dashed line that of [25].

choice of parameters is shown in Fig. 8b and is in good agreement with the parameterisation given in [22].

As well as the different choice for the resonances contributing to the various decay modes this model differs from that of [30] in the treatment of the K_1 resonances. While the model of [30] assumes that only the $K_1(1400)$ contributes the model of [25] assumes that both the $K_1(1270)$ and $K_1(1400)$ contribute with different relative contributions to modes including $K^* \pi$ and $K \rho$ intermediate states. All the parameters are taken from [25].

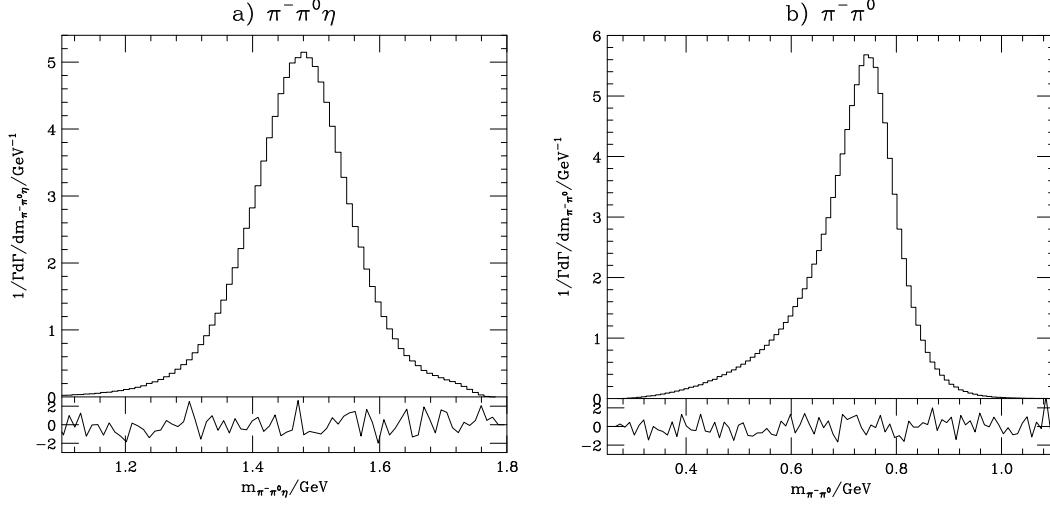


Fig. 17. Differential distribution for the mass of a) $\pi^- \pi^0 \eta$ and b) $\pi^- \pi^0$ produced in the decay $\tau^- \rightarrow \pi^- \pi^0 \eta \nu_\tau$ for the model of [9,30].

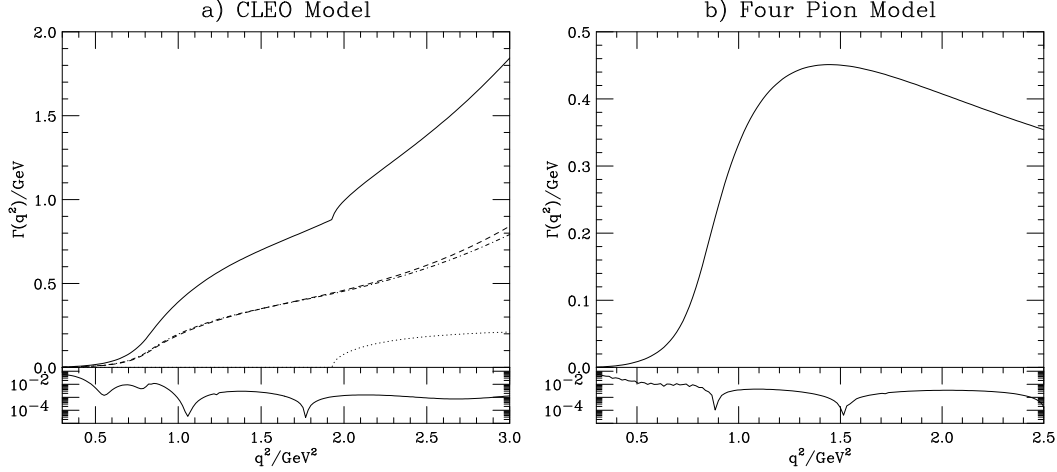


Fig. 18. Running width of the a_1 in the models of [31] and [32]. a) shows the running width in the model of [31] with the dotted line showing the contribution of KK^* , the dashed line showing the contribution of $\pi^- \pi^- \pi^+$, the dot-dashed line showing the contribution of $\pi^0 \pi^0 \pi^-$ and the solid line the total running width. b) shows the running width in the model of [32].

The mass distributions for the total hadronic mass and the mass of the $\pi^- K^+$ subsystem are shown in Fig. 11 for the decay $\tau^- \rightarrow K^- \pi^- K^+ \nu_\tau$. The mass distributions for the total hadronic mass and the mass of the $\pi^- \bar{K}^0$ system is shown in Fig. 12 for the decay $\tau^- \rightarrow K^0 \pi^- \bar{K}^0 \nu_\tau$. The only major difference with the model of [30] for these decay modes is due to the different parameters for the a_1 and the inclusion of higher K^* resonances. The mass distributions for the hadronic system and the $K^- \pi^0$ subsystem for the decay $\tau^- \rightarrow K^- \pi^0 K^0 \nu_\tau$ are shown in Fig. 13. In this case the model of [25] includes K^* resonances in the $K^- \pi^0$ and $\pi^0 K^0$ subsystems which are not presented in the model of [30] giving different results for the masses of these systems and leading to a higher

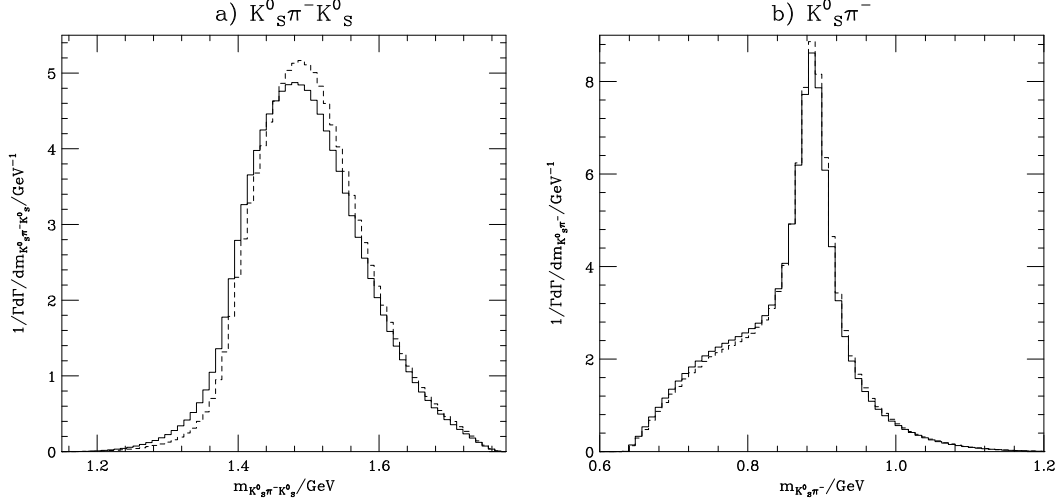


Fig. 19. Differential distribution for the mass of a) $K_S^0\pi^-K_S^0$ and b) $K_S^0\pi^-$ produced in the decay $\tau^- \rightarrow K_S^0\pi^-K_S^0\nu_\tau$. The solid line is the model of [25] and the dashed line is the result of the model of [9,30].

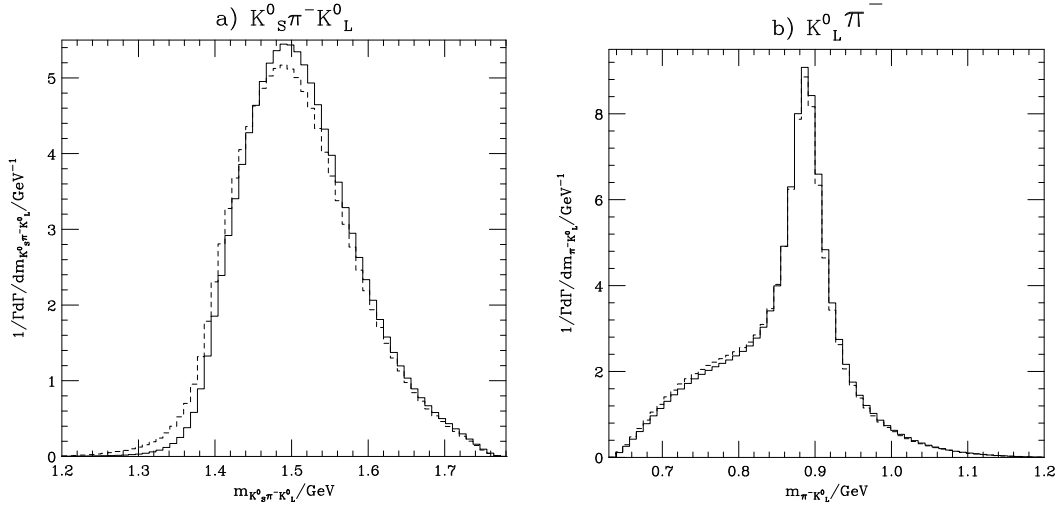


Fig. 20. Differential distribution for the mass of a) $K_S^0\pi^-K_L^0$ and b) $K_L^0\pi^-$ produced in the decay $\tau^- \rightarrow K_S^0\pi^-K_L^0\nu_\tau$. The solid line is the model of [25] and the dashed line is the result of the model of [9,30].

total hadronic mass for this decay mode.

The mass distributions of the hadronic system and the $\pi^0 K^-$ subsystem in the decay $\tau^- \rightarrow \pi^0\pi^0 K^- \nu_\tau$ are shown in Fig.14. In this case the main difference between the models of [25] and [30] is due to the inclusion of the $K_1(1270)$ in the model of [25] which gives the two peak structure seen in the hadronic mass spectrum. The mass distributions for the hadronic system and the $\pi^+\pi^-$ subsystem for the decay $\tau^- \rightarrow K^-\pi^-\pi^+\nu_\tau$ are shown in Fig.15. As with the $\pi^0\pi^0 K^-$ the inclusion of the $K_1(1270)$ gives a different spectrum for the mass of the hadronic system when compared with that from the model of

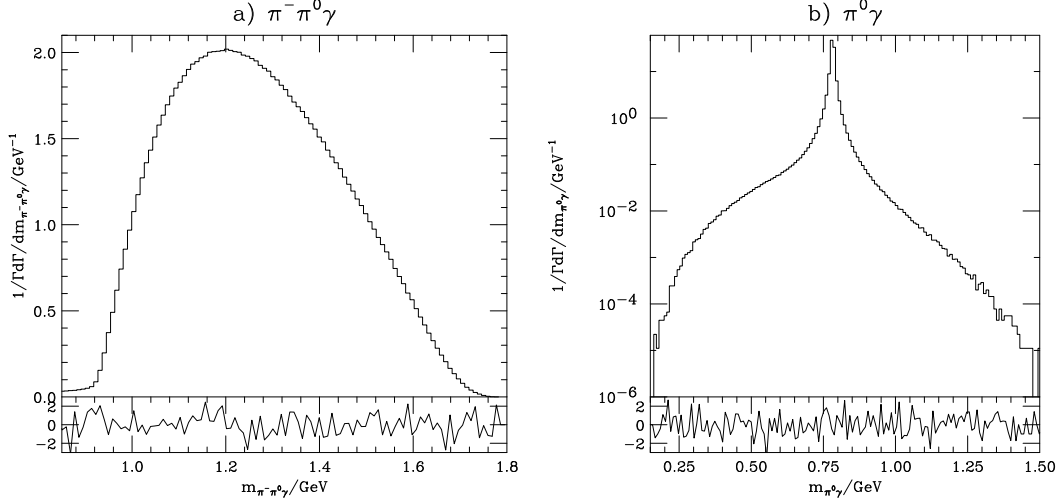


Fig. 21. Differential distribution for the mass of a) $\pi^- \pi^0 \gamma$ and b) $\pi^- \gamma$ produced in the decay $\tau^- \rightarrow \pi^- \pi^0 \gamma \nu_\tau$ for the model of [9].

[30]. The CLEO measurement of this mode [33] favours a significant $K_1(1270)$ contribution but with a much larger width than the model of [25] for the K_1 .

The mass distributions for the hadronic system and the $\pi^- \bar{K}^0$ subsystem for the decay $\tau^- \rightarrow \pi^- \bar{K}^0 \pi^0 \nu_\tau$ are shown in Fig. 16. As with the $K^- \pi^0 K^0$ the presence of K^* resonances in the $\pi^- \bar{K}^0$ and $\bar{K}^0 \pi^0$ systems give a different mass distribution for these systems, which together with the inclusion of the $K_1(1270)$ gives the different result for the mass of the hadronic system.

The mass distribution for the $K_S^0 \pi^- K_S^0$ and $K_S^0 \pi^-$ systems in the decay $\tau^- \rightarrow K_S^0 \pi^- K_S^0 \nu_\tau$ are shown in Fig. 19. The mass distribution for the $K_S^0 \pi^- K_L^0$ are $K_L^0 \pi^-$ systems in the decay $\tau^- \rightarrow K_S^0 \pi^- K_L^0 \nu_\tau$ are shown in Fig. 20. The results from the model of [9,30] are also shown, where the K^0 and \bar{K}^0 are allowed to decay with equal probability to K_S^0 and K_L^0 without changing the hadronic current.⁶ The models are in reasonable agreement for the shapes of these distributions.

3.7 Two Pions and a Photon

The branching ratio for the decay $\tau^- \rightarrow \omega \pi^- \nu_\tau$ is 1.95% [34]. The majority of this decay is modelled as an intermediate state in the four pion current described below. However there is a 8.90% [34] branching ratio of the ω into $\pi^0 \gamma$ which must also be modelled. We do this using a current for $\pi^\pm \pi^0 \gamma$ via an intermediate ω . The hadronic current for this mode, together with the masses, widths and other parameters, are taken from [9].

⁶ The dashed lines in Figures 19 and 20 are therefore identical.

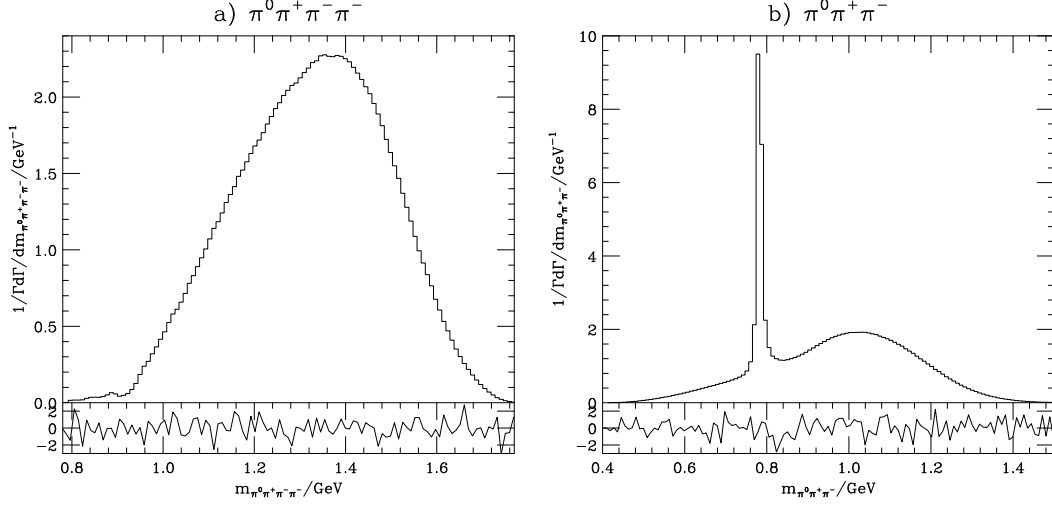


Fig. 22. Differential distribution for the mass of a) $\pi^0\pi^+\pi^-\pi^-$ and b) $\pi^0\pi^+\pi^-$ produced in the decay $\tau^- \rightarrow \pi^0\pi^+\pi^-\pi^-\nu_\tau$ for the model of [32].

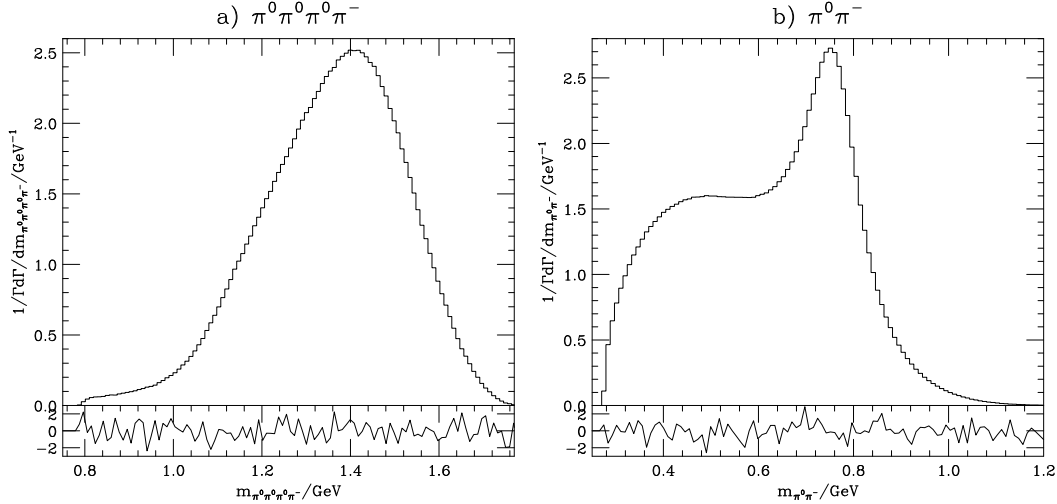


Fig. 23. Differential distribution for the mass of a) $\pi^0\pi^0\pi^0\pi^-$ and b) $\pi^0\pi^-$ produced in the decay $\tau^- \rightarrow \pi^0\pi^0\pi^0\pi^-\nu_\tau$ for the model of [32].

The partial width for the $\tau^- \rightarrow \pi^0\pi^-\gamma$ mode is given in Table. 2. The mass distributions of the hadronic system and the $\pi^0\gamma$ subsystem, which contains the ω resonance, are given in Fig. 21. There is good agreement between **Herwig++** and **TAUOLA** for both the partial width and the shapes of the distributions.

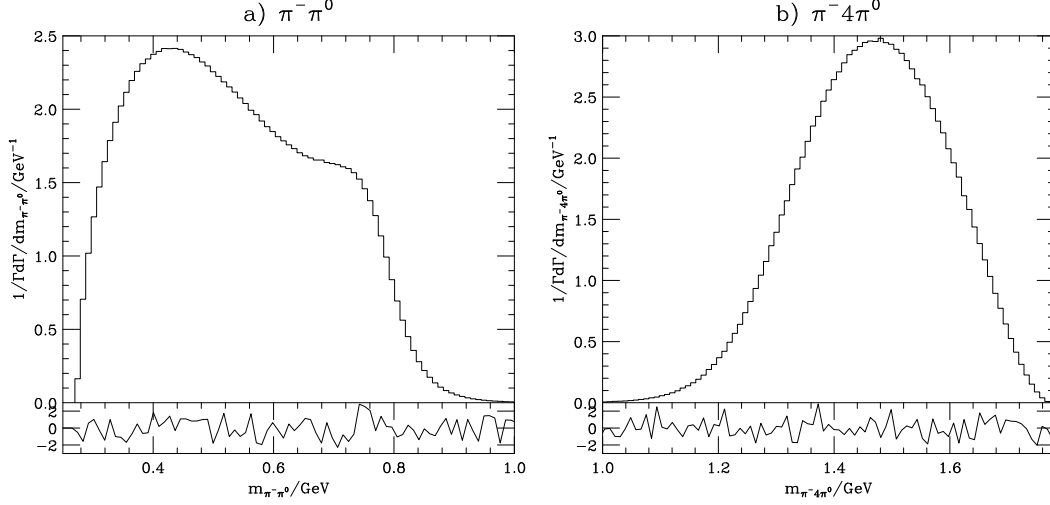


Fig. 24. Differential distribution for the mass of a) $\pi^- \pi^0$ and b) $\pi^- 4\pi^0$ produced in the decay $\tau^- \rightarrow 4\pi^0 \pi^- \nu_\tau$ for the model of [35].

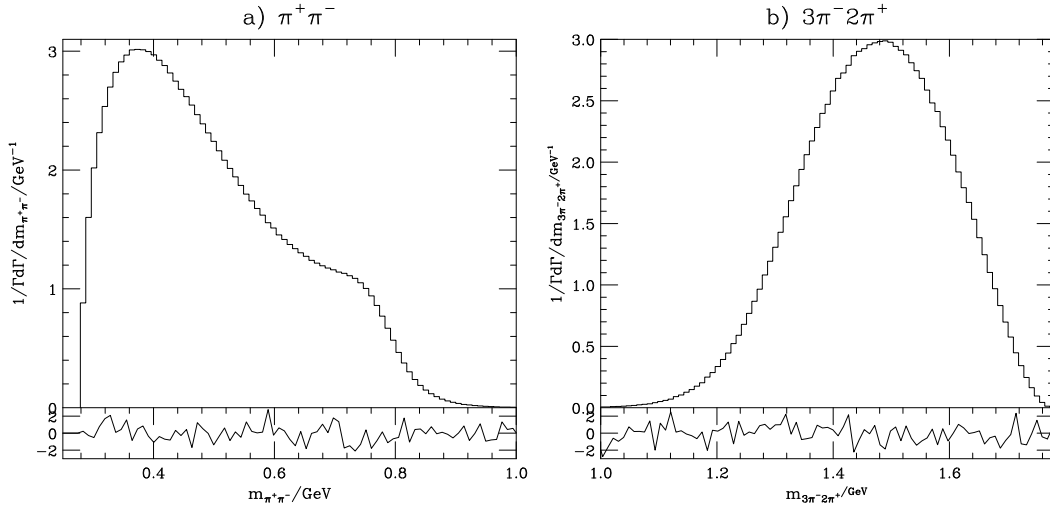


Fig. 25. Differential distribution for the mass of a) $\pi^+ \pi^-$ and b) $3\pi^- 2\pi^+$ produced in the decay $\tau^- \rightarrow 3\pi^- 2\pi^+ \nu_\tau$ for the model of [35].

3.8 Four Pions

We use the model of [32]⁷ to model the decay of the τ to four pions. The model is based on a fit to e^+e^- data from Novosibirsk. A Breit-Wigner distribution with a running width, Eqn. A.2, is used for the σ and ω resonances with the running widths taken from [10]. The more complicated form of [10] is used for the ρ which, apart from the choice to normalise to -1 at $q^2 = 0$, is the same as the form of [23] given in Eqn. A.4.

⁷ It should be noted that there were a number of mistakes in this paper which were corrected in [10].

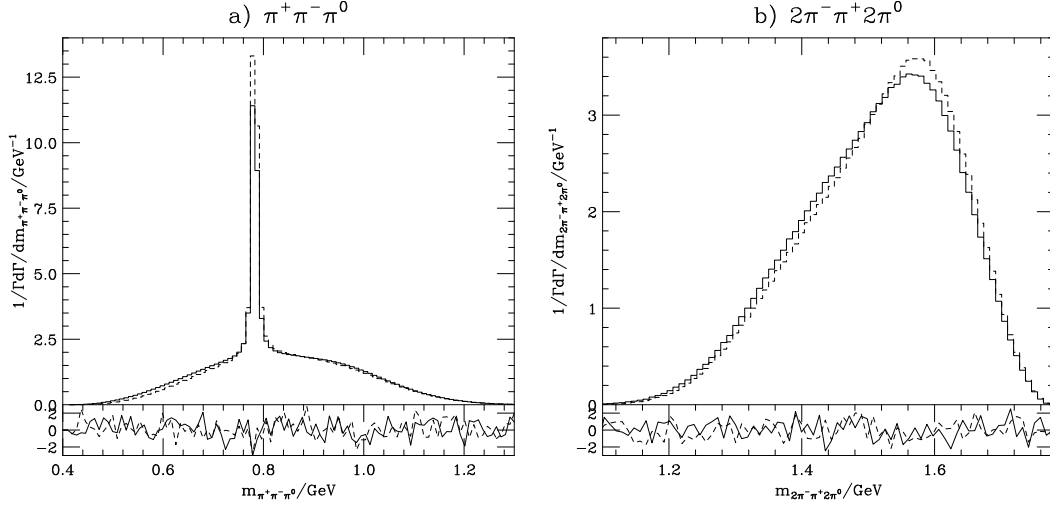


Fig. 26. Differential distribution for the mass of a) $\pi^+\pi^-\pi^0$ and b) $2\pi^-\pi^+2\pi^0$ produced in the decay $\tau^- \rightarrow 4\pi^0\pi^-\nu_\tau$. The solid line is the model of [35] neglecting the ρ propagators in the ω decay and the dashed line includes these propagators, by default we do not include the ρ propagators.

A Breit-Wigner distribution with a running width is used for the a_1 with the running width calculated in [32]. The **Herwig++** calculation of the running width is compared with that from **TAUOLA** in Fig. 18b. There is reasonable agreement between the two calculations apart from in the threshold region.

The partial widths for the two modes are given in Table 2. The mass distributions for the hadronic system and the $\pi^0\pi^+\pi^-$ subsystem, which contains the ω resonance, are shown in Fig. 22 for the decay $\tau^- \rightarrow \pi^0\pi^+\pi^-\pi^-\nu_\tau$. The mass distributions for the hadronic system and the $\pi^0\pi^-$ subsystem are shown in Fig. 23 for the decay $\tau^- \rightarrow \pi^0\pi^0\pi^0\pi^-\nu_\tau$. There is good agreement between **Herwig++** and **TAUOLA** for both the partial widths and mass distributions.

3.9 Five pions

We use the model of [35] which includes $\rho\omega$ and $\rho\sigma$ intermediate states, via the a_1 meson to model the five pion decay modes of the τ .

The partial widths for these decay modes are compared with those from **TAUOLA** in Table 2. The mass distributions of the $\pi^-\pi^0$ subsystem and the hadronic system are shown in Fig. 24 for the decay $\tau^- \rightarrow 4\pi^0\pi^-\nu_\tau$. The mass distributions of the $\pi^+\pi^-$ subsystem and the total hadronic mass for the decay $\tau^- \rightarrow 3\pi^-2\pi^+\nu_\tau$ are shown in Fig. 25. The mass distributions of the $\pi^+\pi^-\pi^0$ subsystem, which includes the ω resonance, and the total hadronic system are shown for the decay $\tau^- \rightarrow 2\pi^-2\pi^0\pi^+\nu_\tau$ are shown in Fig. 26. In all cases there is good agreement between the results of **Herwig++** and **TAUOLA** for both the

partial widths and the shapes of the distributions.⁸

4 Modelling of Tau Decays

In our approach the branching ratios for a given decay mode are specified as input parameters rather than calculated from the theoretical models used to give the distributions of the decay products, which gives us the ability to adjust the branching ratios to the experimentally-observed values. In general we have taken the decay modes and branching ratios for tau decays from [34]. In [34] a set of basis modes is used, the branching ratios for which are constrained to sum to unity. In most cases we have used these modes. However, in some cases due to our modelling of the decays we have combined modes. We have also included some of the non-basis modes, which forces us to adjust the branching ratios slightly from those in [34] in order to ensure that the branching ratios still sum to one. For the higher multiplicity modes where charged hadrons are observed, but the different rates for kaons and pions are not known, we assume that the hadrons are pions. The decay modes, branching ratios and currents used are summarized in Table 3. In addition we have chosen to use the masses from [34] for the external particles, although we use the default choice of the models we are using, which often come from experimental fits, for the intermediate resonances.

The branching ratios for the leptonic modes are taken from [34] and the distribution of the decay products is modelled using the `LeptonNeutrinoCurrent` described in Section 3.3. The decays to a single charged meson are modelled using the `ScalarMesonCurrent`, described in Section 3.1, with the branching ratios taken from [34]. The $K\pi$ modes are modelled using `KPiCurrent`, described in Section 3.5, and the parameters from the fit of [24]. The remaining two meson modes are modelled using the `TwoMesonRhoKStarCurrent`, described in Section 3.4, and the branching ratios from [34], the resonance parameters for the different modes are described in Section 3.4.

The three-pion modes are modelled using the `ThreePionCLEOCurrent`, as described in Section 3.6.2, together with the branching ratios from [34]. We take the branching ratios for modes with three mesons, at least one of which is a kaon, from [34] and use the `KaonThreeMesonCurrent`, as described in Section 3.6.3, to model the distribution of the decay products.

⁸ As the $\omega \rightarrow \pi^+\pi^-\pi^0$ decay is below the threshold for $\rho\pi$ production it can be modeled as either a contact interaction or via the $\rho\pi$ intermediate state. The parameters of [35] are chosen to give the correct relative rates for the different intermediate states without the ρ propagators and we take this as our default choice.

Branching Ratio	Decay Mode	Current
0.178345	$e^- \bar{\nu}_e \nu_\tau$	LeptonNeutrinoCurrent
0.173545	$\mu^- \bar{\nu}_\mu \nu_\tau$	LeptonNeutrinoCurrent
0.108924	$\pi^- \nu_\tau$	ScalarMesonCurrent
0.006885	$K^- \nu_\tau$	ScalarMesonCurrent
0.254890	$\pi^- \pi^0 \nu_\tau$	TwoMesonRhoKStarCurrent
0.008957	$\bar{K}^0 \pi^- \nu_\tau$	KPiCurrent
0.004491	$K^- \pi^0 \nu_\tau$	KPiCurrent
0.001513	$K^- K^0 \nu_\tau$	TwoMesonRhoKStarCurrent
0.000263	$\eta K^- \nu_\tau$	TwoMesonRhoKStarCurrent
0.092370	$\pi^- \pi^0 \pi^0 \nu_\tau$	ThreePionCLEOCurrent
0.089813	$\pi^- \pi^+ \pi^- \nu_\tau$	ThreePionCLEOCurrent
0.003757	$\bar{K}^0 \pi^- \pi^0 \nu_\tau$	KaonThreeMesonCurrent
0.003292	$K^- \pi^- \pi^+ \nu_\tau$	KaonThreeMesonCurrent
0.000555	$K^- \pi^0 \pi^0 \nu_\tau$	KaonThreeMesonCurrent
0.001519	$K^- K^+ \pi^- \nu_\tau$	KaonThreeMesonCurrent
0.001518	$K^- K^0 \pi^0 \nu_\tau$	KaonThreeMesonCurrent
0.001087	$K_L^0 K_S^0 \pi^- \nu_\tau$	KaonThreeMesonCurrent
0.000235	$K_L^0 K_L^0 \pi^- \nu_\tau$	KaonThreeMesonCurrent
0.000235	$K_S^0 K_S^0 \pi^- \nu_\tau$	KaonThreeMesonCurrent
0.044435	$\pi^- \pi^+ \pi^- \pi^0 \nu_\tau$	FourPionNovosibirskCurrent
0.010313	$\pi^- \pi^0 \pi^0 \pi^0 \nu_\tau$	FourPionNovosibirskCurrent
0.001762	$\pi^- \pi^0 \gamma \nu_\tau$	TwoPionPhotonCurrent
0.004935	$\pi^- \pi^- \pi^+ \pi^0 \pi^0 \nu_\tau$	FivePionCurrent
0.001744	$\eta \pi^- \pi^0 \nu_\tau$	ThreeMesonDefaultCurrent
0.000957	$\pi^- \pi^0 \pi^0 \pi^0 \pi^0 \nu_\tau$	FivePionCurrent
0.000834	$\pi^- \pi^- \pi^- \pi^+ \pi^+ \nu_\tau$	FivePionCurrent
0.000225	$\eta \pi^- \pi^- \pi^+ \nu_\tau$	Phase Space
0.000145	$\eta \pi^- \pi^0 \pi^0 \nu_\tau$	Phase Space
0.000135	$\omega \pi^- \pi^0 \pi^0 \nu_\tau$	Phase Space
0.000118	$\omega \pi^- \pi^- \pi^+ \nu_\tau$	Phase Space
0.000400	$K^- \omega \nu_\tau$	Phase Space
0.000397	$K^- \pi^0 \pi^0 \pi^0 \nu_\tau$	Phase Space
0.000307	$K^- \pi^+ \pi^- \pi^0 \nu_\tau$	Phase Space
0.000280	$\eta K^{*-} \nu_\tau$	Phase Space
0.000238	$\bar{K}^0 \pi^- \pi^0 \pi^0 \nu_\tau$	Phase Space
0.000225	$\bar{K}^0 \pi^- \pi^- \pi^+ \nu_\tau$	Phase Space
0.000297	$K^0 \bar{K}^0 \pi^- \pi^0 \nu_\tau$	Phase Space
0.000059	$K^- K^+ \pi^- \pi^0 \nu_\tau$	Phase Space

Table 3

Decay modes and branching ratios used for τ decays in Herwig++ together with the model of the hadronic current used for the decay.

We split the observed $\tau^- \rightarrow \omega\pi\nu_\tau$ rate into its dominant pieces, i.e. $\omega \rightarrow \pi^+\pi^-\pi^0$ and $\omega \rightarrow \pi^0\gamma$. The three pion mode is included with the rest of the four pion tau decays and is modelled using the `FourPionNovosibirskCurrent`, described in Section 3.8, whereas the $\pi^0\gamma$ is modelled using the `TwoPionPhotonCurrent`, described in Section 3.7. The branching ratios are taken from [34]. In general the treatment of non-dominant modes is often a problem when we include resonances as intermediate particles in the hadronic currents. However, in the other cases, such as the ω component to the five pion decays, the contribution of the other modes is smaller and comparable with other neglected tau decay modes and is not included.

The five pion decays for the tau are modelled using the `FivePionCurrent`, described in Section 3.9. As with the four-pion modes we include the ω contribution with the rest of the five-pion modes as the current includes modelling of the intermediate ω contribution. In this case we neglect the sub-dominant ω modes due to their smaller contribution. The branching ratios are taken from [34].

The inclusion of the $\eta 3\pi$ and $\omega 3\pi$ modes is sufficient to saturate the observed six pion rates from [34] and we therefore include these modes using a phase-space distribution for the decay products.

We also include a number of modes with one kaon and three pions, or two kaons and two pions and $K^*\eta$ using a phase-space distribution for the decay products and the branching ratios from [34]. The largest branching ratio for one of these modes is $K\omega$ with a branching ratio of 0.0004 and the sum of the branching ratios for these modes is less than three per mille. This means that they make a relatively small contribution and if necessary the simulation can be improved by implementing hadronic currents for these modes.

As the decay modes, the decay models and branching ratios are specified in a data file these can easily be changed given new experimental results or better modelling of the hadronic currents.

5 Other Applications

The hadronic currents obtained from τ decay can be used to describe other decays which occur via the weak current. It is an important test of the new structure of decays and weak currents in `Herwig++` that the currents can be used to simulate these decays.

One obvious application is to use the currents, together with the naïve factorization approximation, to simulate the weak hadronic decays of bottom and

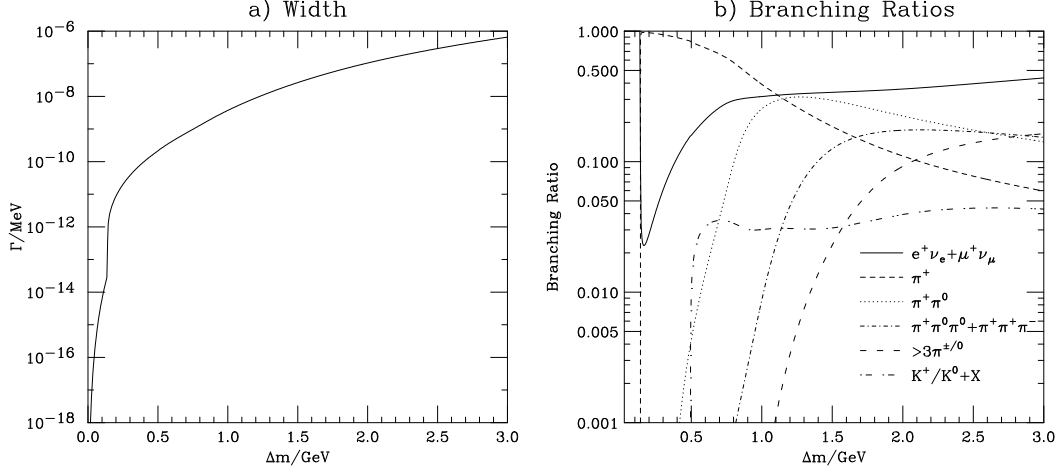


Fig. 27. The a) width and b) branching ratios of the chargino as a function of the mass difference between the chargino and lightest neutralino. The solid line shows the sum of the leptonic modes, *i.e.* $\chi_1^+ \rightarrow \chi_1^0 e^+ \nu_e$ and $\chi_1^+ \rightarrow \chi_1^0 \mu^+ \nu_\mu$. The dashed line shows the pion mode $\chi_1^+ \rightarrow \chi_1^0 \pi^+$ and the dotted shows the $\chi_1^+ \rightarrow \chi_1^0 \pi^+ \pi^0$ mode. The dot-dashed line shows the sum of the $\chi_1^+ \rightarrow \chi_1^0 3\pi$ modes. The long dashed line shows the sum of $\chi_1^+ \rightarrow \chi_1^0 \{4, 5\} \pi$, $\chi_1^+ \rightarrow \chi_1^0 \pi^+ \pi^0 \gamma$, and $\chi_1^+ \rightarrow \chi_1^0 \pi^+ \pi^0 \eta$ modes. The long dot-dashed line shows the sum of the modes involving kaons.

charm hadrons.⁹ Here we will consider another possible use of these currents, the simulation of the weak decay of BSM particles where there is a small mass difference between two of the particles. One such example of this is the decay of the lighter chargino, which is almost mass degenerate with the lightest neutralino, in AMSB models. In most studies of these models only the leptonic and single-pion modes are included, in some more sophisticated studies the two- and three-pion modes were also considered [37,38].

Using the hadronic currents from tau decays it is easy to extend the simulation of BSM decays in [15] to automatically calculate the partial widths and branching ratios for decays with $X \rightarrow YW^\pm$ where the W^\pm is highly off-shell. These decays are calculated by using the `Vertices` for the BSM model, which encode the Feynman rules, and the hadronic current. The partial widths are normalised in order to give the correct branching ratios for the τ with the modes which are modelled using a phase-space distribution neglected. This is a reasonable approximation given the relatively small contribution of these modes. As the partial widths depend on both the overall mass scale, as well as the mass difference, the branching ratios, while often close to, are not necessarily the same as those of the τ when the mass difference is equal to the tau mass. In practice, this approach is normally only used for small values of the mass splitting and matched to the perturbative calculation with outgoing quarks at a mass difference below the charm threshold.

⁹ We will use this approach in the simulation of hadronic decays in `Herwig++` [36].

We illustrate this by considering the decay $\chi_1^+ \rightarrow \chi_1^0 X$ at the AMSB parameter point SPS9 [39]. The SUSY parameters were generated using SOFTSUSY [40]. The mass difference between the lightest neutralino and chargino is very sensitive to higher-order corrections, this can be seen by the large difference between the values obtained using SOFTSUSY (1.167 GeV) and ISAJET7.58 [41] (0.167 GeV), which was used in [39]. Given the uncertainty in the mass difference, and to show dependence of the results upon it, we present the width and branching ratios as a function of the mass difference, Fig. 27, between the neutralino and chargino by keeping all the other SUSY parameters fixed to the values given by SOFTSUSY and varying the chargino mass. As can be seen, for larger values of the mass difference the multi-pion modes (> 3 pions) dominate, although at lower values they typically make a small contribution.

6 Conclusion

We have described the simulation of tau decays in the Herwig++ event generator. A number of tests of the simulation have been performed giving us confidence in the implementation of the various hadronic currents and accuracy of the simulation.

This new simulation makes use of the factorization of the matrix element and the inheritance mechanism of C++ to produce a simulation which is easy to extend by implementing new hadronic currents. The interface feature of the ThePEG framework [6], on which Herwig++ is based, allows easy access to all the parameters of the hadronic currents, allowing different experimental fits to be used without changing any code.

The range of hadronic currents that are included together with the simulation of spin correlation effects in all tau decays gives a state-of-the-art description of tau decays. The new code structure will make this simulation easy to maintain and develop in the future.

Acknowledgments

We are grateful to the other members of the Herwig++ collaboration for both their contributions to the development of the program which underlies this work and many useful discussions. This work was supported by Science and Technology Facilities Council, formally the Particle Physics and Astronomy Research Council, and the European Union Marie Curie Research Training Network MCnet under contract MRTN-CT-2006-035606.

A Breit-Wigner Distributions

A number of different forms of the Breit-Wigner distribution are used in the various hadronic currents. The simplest form of the distribution, which is rarely used, is a fixed width Breit-Wigner distribution

$$B(s) = \frac{M^2 - iM\Gamma}{M^2 - s - iM\Gamma}, \quad (\text{A.1})$$

where s is the virtual mass squared of the resonance, M is the mass of the resonance and Γ is the width. As with many of the forms we use, this is designed so that $B(0) = 1$.

In most cases we make use of a more sophisticated form including a running width for the particle, $\Gamma(s)$:

$$\text{BW}(s) = \frac{M^2}{M^2 - s - i\sqrt{s}\Gamma(s)}, \quad (\text{A.2})$$

The details of this form of the Breit-Wigner distribution depend on the choice of the running width. If the decays of the resonance are dominated by a simple two-body decay, the running width is given by

$$\Gamma^{\text{s-wave}}(s) = \Gamma \frac{M^2}{s} \frac{p(s)}{p(M^2)}, \quad (\text{A.3a})$$

$$\Gamma^{\text{p-wave}}(s) = \Gamma \frac{M^2}{s} \left(\frac{p(s)}{p(M^2)} \right)^3, \quad (\text{A.3b})$$

$$\Gamma^{\text{d-wave}}(s) = \Gamma \frac{M^2}{s} \left(\frac{p(s)}{p(M^2)} \right)^5, \quad (\text{A.3c})$$

where Γ is the physical width and $p(s)$ is the momentum for the 2-body decay of a particle of virtual mass s in the rest frame of the particle. The angular momentum of the decay products is denoted as s-, p-, and d-wave for spin 0, 1, and 2 systems. For particles where the dominant decay is a three-body mode, for example the a_1 meson, a more complicated form of the running width is often used. In this case we still have $\text{BW}(0) = 1$, as the running width is zero below the threshold for the decay modes.

In some cases for the ρ meson we use the form of Gounaris and Sakurai [23], which includes a running mass correction derived from an effective range for-

mula for the p-wave $\pi\pi$ scattering phase,

$$\text{BW}(s) = \frac{M^2 + dM\Gamma}{M^2 - s + \Gamma \frac{M^2}{k_M^3} \{k_s^2 [h(s) - h(M^2)] + k_M^2 h'(M^2)(M^2 - s)\} - iM\Gamma \left(\frac{k_s}{k_M}\right)^3 \frac{M}{\sqrt{s}}} \quad (\text{A.4})$$

where M is the mass of the ρ and Γ is its width. The function $k(s)$ is defined to be

$$k(s) = \sqrt{\frac{1}{4}s - m_\pi^2} \quad s \geq 4m_\pi^2 \quad (\text{A.5a})$$

$$= i\sqrt{m_\pi^2 - \frac{1}{4}s} \quad s < 4m_\pi^2, \quad (\text{A.5b})$$

where we have used $k_M = k(M^2)$ and $k_s = k(s)$ in the definition of the Breit-Wigner distribution. The function $h(s)$ is taken to be

$$h(s) = \frac{2}{\pi} \frac{k}{\sqrt{s}} \ln \left(\frac{\sqrt{s} + 2k}{2m_\pi} \right) \quad s \geq 4m_\pi^2 \quad (\text{A.6a})$$

$$= i \frac{2}{\pi} \frac{k}{\sqrt{s}} \cot^{-1} \sqrt{\frac{s}{4m_\pi^2 - s}} \quad s < 4m_\pi^2, \quad (\text{A.6b})$$

and $h'(s) = \frac{dh}{ds}$. The constant d

$$d = \frac{3}{\pi} \frac{m_\pi^2}{k_M^2} \ln \left(\frac{M + 2k_M}{2m_\pi} \right) + \frac{M}{2\pi k_M} - \frac{m_\pi^2 M}{\pi k_M^3} \quad (\text{A.7})$$

is defined to give $\text{BW}(0) = 1$.

References

- [1] P. Richardson, JHEP 11 (2001) 029, hep-ph/0110108.
- [2] S. Catani et al., JHEP 11 (2001) 063, hep-ph/0109231.
- [3] S. Frixione and B.R. Webber, JHEP 06 (2002) 029, hep-ph/0204244.
- [4] S. Gieseke, P. Stephens and B. Webber, JHEP 12 (2003) 045, hep-ph/0310083.
- [5] P. Nason, JHEP 11 (2004) 040, hep-ph/0409146.
- [6] M. Bertini, L. Lönnblad and T. Sjöstrand, Comput. Phys. Commun. 134 (2001) 365, hep-ph/0006152. L. Lönnblad, Nucl. Instrum. Meth. A502 (2003) 549.

- [7] S. Gieseke et al., JHEP 02 (2004) 005, hep-ph/0311208. S. Gieseke et al., (2006), hep-ph/0609306. M. Gigg and P. Richardson, (2007), arXiv:0706.2921 [hep-ph].
- [8] T. Gleisberg et al., JHEP 02 (2004) 056, hep-ph/0311263.
- [9] S. Jadach et al., Comput. Phys. Commun. 76 (1993) 361.
- [10] P. Golonka et al., (2003), hep-ph/0312240.
- [11] I.G. Knowles, Nucl. Phys. B310 (1988) 571.
- [12] I.G. Knowles, Comput. Phys. Commun. 58 (1990) 271.
- [13] J.C. Collins, Nucl. Phys. B304 (1988) 794.
- [14] Z. Wąs and M. Worek, Acta Phys. Polon. B33 (2002) 1875, hep-ph/0202007.
- [15] M. Gigg and P. Richardson, (2007), hep-ph/0703199.
- [16] K. Desch, Z. Wąs and M. Worek, Eur. Phys. J. C29 (2003) 491, hep-ph/0302046.
- [17] K. Hamilton and P. Richardson, JHEP 07 (2006) 010, hep-ph/0603034.
- [18] D.R. Yennie, S.C. Frautschi and H. Suura, Ann. Phys. 13 (1961) 379.
- [19] CLEO, S. Anderson et al., Phys. Rev. D61 (2000) 112002, hep-ex/9910046.
- [20] Belle, K. Abe et al., (2005), hep-ex/0512071.
- [21] ALEPH, S. Schael et al., Phys. Rept. 421 (2005) 191, hep-ex/0506072.
- [22] J.H. Kühn and A. Santamaria, Z. Phys. C48 (1990) 445.
- [23] G.J. Gounaris and J.J. Sakurai, Phys. Rev. Lett. 21 (1968) 244.
- [24] Belle, D. Epifanov et al., (2007), arXiv:0706.2231 [hep-ex].
- [25] M. Finkemeier and E. Mirkes, Z. Phys. C69 (1996) 243, hep-ph/9503474.
- [26] A. Pich, Phys. Lett. B196 (1987) 561.
- [27] ALEPH, R. Barate et al., Eur. Phys. J. C11 (1999) 599, hep-ex/9903015.
- [28] A.J. Lyon, SLAC-R-785.
- [29] M. Finkemeier and E. Mirkes, Z. Phys. C72 (1996) 619, hep-ph/9601275.
- [30] R. Decker et al., Z. Phys. C58 (1993) 445.
- [31] CLEO, D.M. Asner et al., Phys. Rev. D61 (2000) 012002, hep-ex/9902022.
- [32] A.E. Bondar et al., Comput. Phys. Commun. 146 (2002) 139, hep-ph/0201149.
- [33] CLEO, D.M. Asner et al., Phys. Rev. D62 (2000) 072006, hep-ex/0004002.
- [34] Particle Data Group, W.M. Yao et al., J. Phys. G33 (2006) 1.
- [35] J.H. Kühn and Z. Wąs, (2006), hep-ph/0602162.

- [36] D. Grellscheid, K. Hamilton and P. Richardson, Simulation of Meson Decays in the Herwig++ Event Generator, in preparation.
- [37] C.H. Chen, M. Drees and J.F. Gunion, Phys. Rev. D55 (1997) 330, hep-ph/9607421. C.H. Chen, M. Drees and J.F. Gunion, (1999), hep-ph/9902309.
- [38] A.J. Barr et al., JHEP 03 (2003) 045, hep-ph/0208214.
- [39] B.C. Allanach et al., (2002), hep-ph/0202233.
- [40] B.C. Allanach, Comput. Phys. Commun. 143 (2002) 305, hep-ph/0104145.
- [41] H. Baer et al., (1999), hep-ph/0001086.